Volume 27
Number 48
28 December 2025
Pages 25701–26154

PCCP

Physical Chemistry Chemical Physics

rsc.li/pccp

25 YEARS ANNIVERSARY

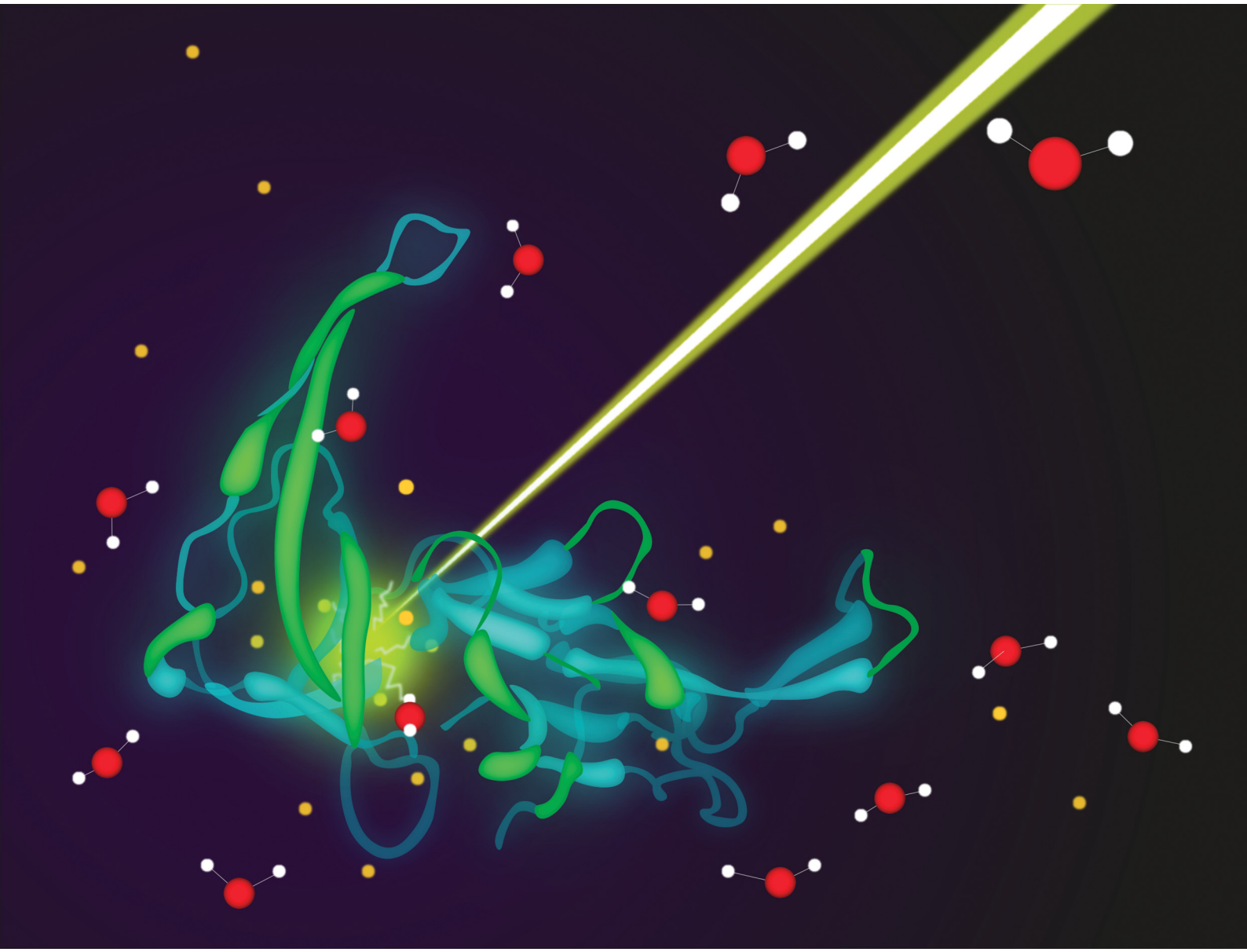

ISSN 1463-9076

ROYAL SOCIETY OF CHEMISTRY

PAPER

Marc Benjamin Hahn *et al.*
Radiation damage to amino acids, peptides and DNA-binding proteins: the influence of water directly monitored by X-ray photoelectron spectroscopy

PCCP Owner Societies

PCCP

ROYAL SOCIETY OF CHEMISTRY

PAPER

View Article Online
View Journal | View Issue

Cite this: *Phys. Chem. Chem. Phys.*, 2025, **27**, 25789

Radiation damage to amino acids, peptides and DNA-binding proteins: the influence of water directly monitored by X-ray photoelectron spectroscopy

Dorothea C. Hallier, [abc] Jörg Radnik, [c] Paul M. Dietrich, [d] Harald Seitz [b] and Marc Benjamin Hahn *[ce]

Ionizing radiation damage to biomolecules plays a crucial role in radiotherapy as a cancer treatment. Among these, DNA-binding proteins are of particular interest due to their pivotal roles in shielding DNA and facilitating its repair. Hence, in this study, we present first-ever recorded data of radiation damage to a protein monitored directly with near-ambient pressure (NAP) X-ray photoelectron spectroscopy (XPS) under a water atmosphere. This surface sensitive technique was used to *in situ* damage and probe gene-V protein (G5P, a model DNA-binding protein) under wet NAP conditions and dry vacuum (UHV) conditions to determine the effect of water on the radiation response. In addition, the X-ray radiation damage to selected pure amino acids and short homopeptides was determined to better understand the variety of damage mechanisms within the complex protein. In dry samples, drastic chemical changes were detected in all biomolecules dominated by fragmentation processes. Here, the breakage of peptide bonds in the peptides and the protein are dominant. Surprisingly, hydration – despite introducing additional indirect damage pathways *via* water radiolysis – led to a reduction in overall radiation damage. This behaviour was attributed to hydration-dependent changes in reaction rates and respective deexcitation and damaging channels within the molecules and secondary species such as low-energy (LEE), (pre)-hydrated/(pre)-solvated electrons and radical species such as hydroxyl radicals.

Received 19th May 2025,
Accepted 20th October 2025

DOI: 10.1039/d5cp01887k

rsc.li/pccp

1 Introduction

When biomolecules are exposed to ionizing radiation, a variety of changes can be observed. This so called radiation damage of biomolecules is the basis for the application of radiation in (radio)-therapy for the treatment of cancer.[1] Here, the damage to the biomolecule DNA, which is the carrier of genetic information, is of major scientific interest, since intact DNA is crucial for the survival of cells.[2] Various studies were performed to investigate the radiation response of this important biomolecule in the past.[3–10]

Today, it is known that another group of biomolecules is of great importance for the cell survival as well: proteins that interact with DNA. They play a central role in the DNA metabolism, for example through participation in DNA replication, recombination and repair. Their presence can protect the DNA against radiation attacks, modify or worsen the respective damage[4–8] and therefore drastically influence the radiation effects on DNA. For example, geometry-dependent shielding of proteins can protect double-stranded DNA (dsDNA) against OH-radical attacks.[11] In contrast to this protective effect, ionizing radiation can lead to the formation of DNA–protein cross-links, which are difficult to repair for the cell.[12]

Due to the distinct influence of the interaction of proteins with DNA on the radiation effects, proteins and DNA–protein complexes present a noteworthy target in radiation research. Therefore it is necessary to investigate the radiation response of proteins – additionally to DNA. The clarification of the underlying molecular mechanisms of radiation damage to complex biomolecules (like proteins) would not only benefit the understanding of the radiation response of (cancerous) cells in radiotherapy but also basic research in other fields like astrobiology. Here, the examination of the influence of radiation on (simple) biomolecules could deliver valuable information and possible explanations for the beginning of life itself. For example, in outer space radiation induced synthesis of the

[a] *Institute of Biochemistry and Biology, University of Potsdam, 14476 Potsdam, Germany*
[b] *Fraunhofer Institute for Cell Therapy and Immunology Branch Bioanalytics and Bioprocesses IZI-BB, 14476 Potsdam, Germany*
[c] *Bundesanstalt für Materialforschung und – prüfung (BAM), 12205 Berlin, Germany*
[d] *SPECS Surface Nano Analysis GmbH, 13355 Berlin, Germany*
[e] *Institute of Chemistry, University of Potsdam, 14476 Potsdam, Germany. E-mail: marc-benjamin.hahn@fu-berlin.de*

elementary building blocks of life (like amino acids) was proposed.[13]

Yet, the processes and underlying molecular mechanisms involved in radiation damage to proteins are not fully understood: proteins are characterized through their chemical and physical properties that cater their stability and activity and ultimately provide their function. Radiation damage can interfere with all these attributes: destabilize and deactivate proteins, cause malfunctions through breakage of molecular bonds, the formation of carbon-centred radicals,[14] inter- or intramolecular cross-linkage,[15] as well as a macroscopic change of the secondary structure, which can all conclusively lead to a change in conformation and most severely a loss of function.

In this study, gene-V protein (G5P/GVP Swissprot P69544) was chosen as the model protein. It belongs to the group of single-stranded DNA binding proteins (SBP), that directly interact with single-stranded DNA (ssDNA).[16–18] When it comes to radiation damage of biomolecules in organisms, this group of proteins is of specific interest. They serve as protectants for ssDNA which is frequently exposed during many cellular processes such as replication, recombination and transcription. SBPs immediately bind to exposed ssDNA to protect it from mutation until the correct biological reaction is completed.[19,20] G5P is a well-investigated biologically-relevant model SBP. A G5P monomer has a molecular weight of 9.7 kDa. Its 87 amino acids are mostly in beta conformation, organized as a five-stranded antiparallel beta-sheet and two antiparallel beta-ladder loops with a broad connecting loop structure[21,22] and its binding behaviour to DNA as a dimer[16–18] was previously determined. G5P's radiation response was previously characterized with other techniques like small-angle X-ray scattering (SAXS).[15] With SAXS, structural changes of G5P upon irradiation were investigated. In contrast, in the present study, chemical changes upon irradiation are investigated. Of about 10 kDa in size, in the biological sense, G5P can be categorized as a small protein, while from a chemical point of view it presents as a large and complex molecule. In addition, in solution G5P can form a dimer. The variety of chemical bonds and the chemical contributions from all 87 single amino acids a G5P monomer consists of, make it difficult to analyse G5Ps radiation response. Therefore, in addition to the protein, model amino acids (alanine $C_3H_7NO_2$, arginine $C_6H_{14}N_4O_2$, cysteine $C_3H_7NO_2S$, glycine $C_2H_5NO_2$ and tyrosine $C_9H_{11}NO_3$, structures shown in Fig. 1) were investigated. The lack of a peptide bond in amino acids also required short peptides to be included in this study. This was necessary to determine the radiation effect to the peptide bond in comparison to the pure amino acids without a peptide bond. Due to the previous work on the chemical influence of different amino acids within short heteropeptides by Stevens *et al.*,[23] in this study, only homopeptides consisting of five molecules of either alanine, glycine and tyrosine were studied.

Soft X-rays were used to damage the above mentioned biomolecules by radiation and analyzing them simultaneously with the technique of X-ray photoelectron spectroscopy (XPS), sometimes also called electron spectroscopy for chemical analysis (ESCA). This method allows simultaneous irradiation and damage monitoring of the samples: photoabsorption leads to the emission of primary (photo-)electrons, which then generate secondary electrons through inelastic scattering, ultimately leading to radiation damage. To date, most radiation exposure studies of DNA–protein complexes (with only a few exceptions like the Spotheim-Maurizot *et al.* study from 2010[24]) were performed under artificial environments: at low temperatures, and under vacuum[25] without consideration of the natural biological surroundings like hydration shells of the analytes. The type and spatial distribution of ionizing events differ drastically between artificial environments like vacuum and water:[26] due to the high amount of water in biological tissue, most inelastic scattering processes between incoming high-energy radiation and tissue occur with the solvent.[10,27] In addition to that, ionizing radiation damage is mediated by reactive species generated from water radiolysis. These reactive species, so called secondary products of ionizing radiation, can effectively generate indirect damage. One of the most abundant reactive species upon water radiolysis are oxidizing hydroxyl radicals which cause a major part of reaction-induced reactivity.[11,28–30] Furthermore, pre-hydrated electrons[31,32] and low-energy electrons (LEE)[1,33,34] are considered to be an additional source of damage. Generally, radiation damage can be divided into the already mentioned indirect effects (modifications induced by reactive species like reactive oxygen species (ROS) generated from the solvent) and direct effects caused by ionization, excitation or formation of transient negative ions (TNI), dissociative electron attachment (DEA) *etc.* of the analytes, directly involving the incoming primary radiation or secondary electrons with a kinetic energy above zero electron volt.[2,28,30,34] In addition, quasi-direct effects occur, when indirect effects generate reactive species in direct proximity to the analytes. Here, the initial ionization event is located, at for example a water molecule of the first hydration shell of the analyte, which then directly reacts with the analyte (*e.g.* by transferring an electron or hole) without undergoing reaction with other solvent molecules or cosolutes as it normally would happen in the bulk.[30,35]

The newly developed technique of near-ambient pressure (NAP)-XPS grants the investigation of radiation damage under a

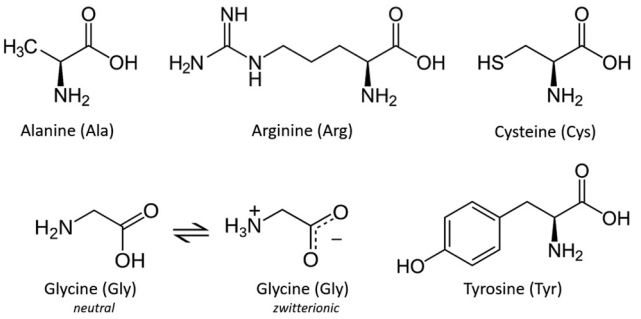

Fig. 1 Chemical structures of the amino acids: alanine, arginine, cysteine, glycine and tyrosine. As an example of the ability of amino acids to exist in different configurations, glycine is displayed in neutral and zwitterionic configuration.

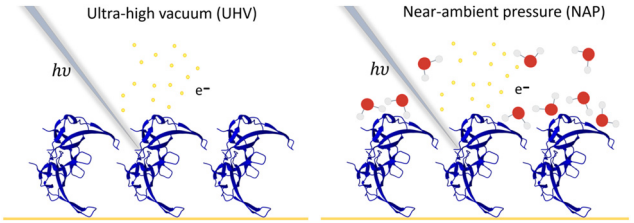

Fig. 2 Sketch of the applied irradiation conditions. X-rays pass though the vacuum (left), absorb at the protein (blue), and/or water (right) atmosphere cause damage and eject photoelectrons. The photoelectrons provide information about the bonds and chemical changes within the molecules and are measured (compare Fig. 3) to monitor damaging processes.

(near-ambient) water atmosphere. During the measurement, a gaseous water atmosphere of 5 mbar is applied above the condensed sample. This allows for (1) a combined monitoring of direct and indirect radiation effects on biomolecules that are hydrated, where direct and indirect radiation damage are caused by inelastic scattering from the target and reactive species, respectively. When these experiments are compared with measurements performed in vacuum, where only direct damage occurs, (2) the disentanglement of direct (through the radiation) and indirect (through reactive species created by water radiolysis, as well as quasi-direct) effects to the biomolecules becomes possible, as described in depth in our previous work.[9] Here, especially the dynamics and reaction ranges of reactive species such as hydroxyl radicals, prehydrated and low-energy electrons are of interest. In this study, we compare direct radiation damage under ultra-high vacuum (UHV, see Fig. 2, left) and direct and indirect radiation damage under NAP conditions on hydrated amino acids, small peptides and G5P protein (see Fig. 2, right). This allows the study of changes of radiation damage yields and the systematic detection of chemical changes caused by radiation in the absence and presence of water on the complex biomolecules.

2 Materials and methods

2.1 Amino acids

Five amino acids were selected: alanine, arginine, cysteine, glycine and tyrosine. They are either one of the most abundant amino acids within G5P (alanine [4× per monomer], glycine [7× per monomer]) or the most important for the bond to DNA (positively charged arginine [4× per monomer] for the interaction with the negatively charged DNA, tyrosine [5× per monomer] with aromatic side chain for interaction with nucleobases) or most likely to be attacked by radiation (due to their sulphur group cysteine [1× per monomer]) and therefore of high relevance for this study even though they are not very abundant in G5P itself.

Pure amino acids L-alanine, L-arginine, L-cysteine, L-glycine and L-tyrosine were obtained from Merck Germany (purity above 99 percent). Amino acids were dissolved in water shortly below their individual solubility limit.

2.2 Peptides

Short peptides consisting of five monomers of alanine, glycine and tyrosine, respectively, were obtained after individual production from Peptide Speciality Laboratories GmbH, Heidelberg, Germany. The peptides were dissolved in water shortly below their individual solubility limit. The small peptides were only studied under UHV conditions.

2.3 Expression and purification of gene-V protein G5P

The G5P (Swissprot: P69544, 87 AA, M_w 9688 Da) plasmid PET-30b was transformed into Xl-1 blue and grown on 2YT agar with 50 μg mL^{-1} Kanamycin. 16 mL overnight culture was inoculated into 1.6 L 2YT medium. Protein expression was induced with 1 mM IPTG at an OD600 = 0.6 for 4 h. Cells were collected, resuspended in 24 mL lysis buffer (PBS with 75 mM NaCl) and sonicated. Cell debris were removed and the supernatant was separated with an ÄKTA FPLC system using a Resource Q anion exchange column (both GE Healthcare, USA). Protein was found in the flow which was purified with 1 mL NiNTA suspension (Qiagen, Netherlands). Resin was washed with 15 mL buffer and protein eluted with 5 mL buffer with 250 mM Imidazole. Protein concentration was determined by BCA assay. A purity of above 95 percent was achieved as determined by SDS–PAGE. Protein was dialysed thoroughly in water. Protein was stored at −20 °C.

2.4 Sample preparation of amino acids, peptides and gene-V protein

The samples – solutions of amino acids, small peptides and the protein – were dropcast onto either SPR gold-on-glass sensorchips obtained from XanTec bioanalytics GmbH (Duesseldorf, Germany) or a gold-coated Si wafer substrate that was produced at BAM Berlin (see affiliation details above) with a SciFLEX ARRAYER S11 (SCIENION GmbH, Berlin, Germany). The spots had an estimated thickness of at least 500 nm, being much longer than the range of LEE from the substrate. The samples were dried under ambient conditions. The spotted wafer and/or sensor chips were stored and transported within evacuated sealing bags, stored and transported at −20 °C until measurement was performed. Before the measurements the samples were left to degas further in the chamber of the XPS system and the procedures are described in the following.

2.5 X-ray photoelectron spectroscopy XPS measurements

2.5.1 Experimental details for ultra-high vacuum conditions.

All XPS measurements under UHV conditions were performed with Al K alpha radiation (E = 1486.6 eV). The UHV-XPS measurements were performed with an ULVAC-Phi Quantes photoelectron spectrometer (Power 24.0 W, Source Size 0.1 mm × 0.1 mm, Spherical Sector Analyzer, 55 eV Analyzer Pass Energy, 0.1 eV step size). Here, the pressure was $<1 \times 10^{-8}$ mbar. The electron emission angle was 45 and the source-to-sample angle was 0 degrees. The binding energy scale of the instrument was calibrated following a procedure which uses ISO 15472 binding energy data.[36] The samples were fixed on double adhesive tape.

Charge compensation with low energy Ar^+ ions and e^- from a flood gun were used. During the UHV measurements the measurement of C 1s, O 1s, N 1s, and S 2p regions took approximately 14 hours for the amino acids and 19 hours for the peptides, respectively. Irradiations were performed continuously for each sample. Only the measurements of the different elements were performed sequentially in alternating order, since the photoelectron detector can only measure photoelectrons with a certain kinetic energy (KE) at once, the same applies for the NAP measurements.

2.5.2 Experimental details for near-ambient pressure conditions. Laboratory NAP-XPS measurements were performed with an EnviroESCA (SPECS GmbH, Berlin, Germany).[37–39] The monochromatic Al Kα X-ray source is separated from the measurement chamber by a silicon nitride window, and the hemispherical energy analyzer is under ultra-high vacuum ($<1 \times 10^{-8}$ mbar) due to a three stage differential pumping system between the analysis section and analyzer. The entrance aperture (nozzle) has a diameter of 300 μm and the usual working distance is 1–2 times the nozzle diameter. With this set-up, it is possible to measure gaseous, liquid as well as solid samples at pressures up to 50 mbar. For ambient pressure measurements samples were inserted into the EnviroESCA and the pressure was slowly reduced below 5 mbar to allow residually dissolved gases to evaporate and be replaced by water molecules. During the NAP-XPS measurements of about 13 hours, the pressure was kept in the near-ambient pressure regime between 4 and 5 mbar as displayed in the pressure curve of the water ambience in the SI Fig. S1. Charge compensation was provided by the presence of the gas atmosphere during NAP measurements. All survey spectra were acquired with a pass energy of 100 eV, a step size of 1.0 eV, and a dwell time of 0.1 seconds. High-resolution core-level spectra (O 1s, N 1s, C 1s, and S 2p) were recorded in fixed analyzer transmission (FAT) mode at a pass energy of 50 eV, a step size of 0.2 eV, and a dwell time of 0.1 seconds. The binding energy scale of the instrument was calibrated according to ISO 15472.[36] The electron emission angle was 0 and the source-to-analyzer angle was 55 degrees.

2.5.3 Analysis of XPS data. Deconvolution of the XPS signals was performed with the Fityk software and a Levenberg–Marquardt algorithm from the MPFIT library.[40] A Shirley background was subtracted from all spectra. The BE values of the spectra measured under UHV and NAP conditions were charge corrected on the C 1s BE at 285 eV. The time dependent evolution and comparisons of the C 1s, N 1s, O 1s and S 2p regions are normalized on the total integrated peak area of the respective time point of each element (the sum is normalized to 100%). The percentage of the intensity in the time dependent figures is given with respect to the total integrated peak area at the beginning of the irradiation. Voigt peaks with a fixed shape of 0.2 (Lorentz–Gauss ratio) were fitted to the spectra based on the assignments from the literature given and summarized in Table 1. The peaks were constrained to a range of ±0.2 eV around their center positions within the same measurement series, either, UHV conditions or H_2O atmosphere. Within each envelope the FWHM was constrained to ±0.05 eV (compare Voigt peak parameters in the SI Tables S1 and S2). The signal contribution from water in the O 1s binding energy region was assigned, based on the work by Patel *et al.*[38] The relative uncertainties for peak area calculation under NAP and UHV conditions were estimated with a matrix inversion approach.[41]

Table 1 Peak assignment and binding energies for UHV and NAP conditions

Element	BE/eV	Bonds
S 2p	163.5	S–C (doublet)
S 2p	164.7–164.8	S–C (singlet)
C 1s	283.6–284.5	C═C
C 1s	285.0	C–C, C–H
C 1s	286.1–286.8	C–O, C–N, C–S
C 1s	288.0–288.6	C═O, O═C–N
C 1s	289.1–289.3	C
N 1s	399.1–399.9	NH_2
N 1s	400.0–400.2	N, O═C–N
N 1s	401.0–401.7	NH_3^+
O 1s	530.5–531.5	C═O, COO^-
O 1s	531.8–532.6	O═C–N
O 1s	532.5–533.4	C–O, –OH, COOH
O 1s	534.0–535.4	H_2O
Na	536.4–536.5	Auger KLL

2.5.4 Estimation of the radiation dose. To estimate the dose in the region of the sample from where the measured photoelectrons originate, particle scattering simulations of the impact of the X-rays onto the sample surfaces were performed, modelling the respective experimental geometries and settings. The particle scattering simulations were performed with the *Geant4* 11.4.1 framework and the O*penTopas* 4.0 interface. The *g4em-livermore* physics-list was enabled with a 1 nm cut length of the particles.[42,43] During the scattering simulations, Auger, AugerCascade and Fluorescence processes were enabled, while multiple-scattering processes were inactive. For a detailed discussion of these settings compare our previous work.[44] 10^8 X-ray photons with 1.487 keV primary energy were simulated to impact the target perpendicular (vacuum conditions) or in an angle of 55° (NAP) to the surface normal, as defined by the experimental geometry. Accordingly, the beam of the vacuums system was modeled with a flat distribution of 100 μm in diameter, while the NAP system with a Gaussian distribution with a standard deviation of about 85 μm was modelled. For both settings under vacuum, or water atmosphere, an independent simulation was performed. The vacuum was modeled with the standard "vacuum" settings, as included in *Topas*, NAP conditions with a temperature of 300 K, a pressure of 2000 Pa and a density of 14.4 μg cm^{-3} for H_2O, were used as a medium, exactly as performed and described previously.[9] The amino acids and proteins were modeled with the predefined material *G4_ALANINE*. The surface layer under NAP conditions was assumed to have 1 nm thickness of water and a density of 1 g cm^{-3}. Dose was calculated in a 10 nm thick layer and a bin size of 1 μm in x and y direction. Based on the simulated dose, the reported photon flux density of the devices of 1.9×10^{10} photons s^{-1} μm^{-2} for the μFOCUS source in the Specs NAP, measured with a photocurrent induced in a GaAs-Diode at 50 W power. Similar values

were obtained for the Phi Quantes XPS system used for the vacuum experiments. Here, a 100 μm diameter beam was measured with a opto-photodiode AXUV100G at 25 W for the Al Kα source, resulting in 7×10^9 photons s^{-1}. These photon flux datasets were used in combination with the simulations results and exposure time, to estimate the dose delivered to the top layer of the sample with 10 nm thickness. Plots of the spatially resolved dose deposit can be found in the SI (Fig. S13 and S14). Since the X-ray spot is much more extended than the acceptance volume of the nozzle in the photo-electron detection system, which is, especially in the NAP system brought as close as possible to the sample surface, to achieve optimal SNR, only photoelectrons originating from the most central and intensely irradiated part contribute to the measured spectra. Therefore we calculated the mean values for the one hundred bins, which received the highest dose, assuming perfect optimization of the nozzle positions during the measurements, to estimate the dose. For the vacuum measurements about 7.5×10^5 kGy were deposited in this region, while for the NAP measurements about 11.9×10^5 kGy were deposited. Since the detector nozzle position varies somewhat between the measurements, the resulting dose values should be regarded as an estimate only, thus the various samples irradiated under both conditions received a dose within the same order of magnitude. Future work should include *in situ* dosimetry to improve on this situation.

3 Results

Here, we present the first simultaneous induction and probing of ionizing radiation damage to amino acids, peptides and proteins by NAP XPS under a water atmosphere as well as standard UHV XPS conditions.

High resolution spectra were obtained at selected time points throughout the ongoing radiation for all elements within the sample (carbon C1s, nitrogen N1s, oxygen O1s and for the samples containing sulphur, sulphur S2p respectively). All of the spectra can be found in the SI. The peaks are assigned to different chemical bonds (see Table 1) based on literature values.[23,45–53] These bonds show a certain chemical shift that is unique for every molecule due to its individual electron configuration and environment. Therefore, the binding energies (BE) can differ in about ±0.3 eV between the amino acids, as well as the peptides and the protein. Thus, a range of BE is given in the overview in Table 1. Generally, the C1s signal is deconvoluted into different peaks for C═C, C–C, C–N, C–O, C–S, and C═O as well as O═C–N, the peptide bonds, respectively. The N 1s spectra are deconvoluted into contributions from amines, NH_3^+ (protonated) and NH_2 (deprotonated) and guanidine (from arginine and G5P protein) as well as O═C–N. Most of the N1s spectra show strong noise (low signal-to-noise ratio (SNR)), which makes fitting and revealing the actual elemental composition difficult. The O1s spectra are deconvoluted into components assigned either to double-bonded oxygen in carboxyl groups, COOH (protonated) and COO^- (deprotonated) as well as O═C–N or single-bonded oxygen from C–O and molecular water H_2O. For peak assignment of S2p sulphur bonds, a doublet separation of $S2p_{3/2}$ and $S2p_{1/2}$ was performed, where S2p BE of 163.5 eV corresponds to $S2p_{3/2}$ and 164.7–164.8 eV corresponds to $S2p_{1/2}$, respectively.

In the following, the UHV results are presented and compared with previous studies. Then, the NAP results and the respective modifications of the underlying damaging channels by the presence of water atmosphere are presented.

3.1 Direct radiation damage under standard UHV conditions

3.1.1 Amino acids. Amino acids are the building blocks of proteins and consist of an amino group, a carboxyl group and an additional side-chain bound to a central C-atom (also named alpha-C). Glycine is the simplest amino acid since it contains no side chains other than H-atoms (see the structure in Fig. 1). Several radiation studies have shown that the side-chain of amino acids plays a special role in the charge distribution and possibly the resulting damage upon irradiation.[54,55] Alanine can be considered the simplest amino acid with a side chain of one CH_3 group. Therefore, alanine was chosen as a model amino acid on the basis of which the processes of radiation damage in XPS are to be described in detail. In Fig. 3, the XPS spectra of alanine under vacuum conditions at C1s, O1s and N1s BE are shown for the beginning (Fig. 3 top row) and end (Fig. 3 centre row) of the X-ray exposure. In the beginning, in the C1s spectrum, three peaks can be determined at 285.0, 286.7 and 288.2 eV, that can be assigned to C–C, C–N and C–O bonds as well as the C in the carboxyl-group, respectively. An additional peak at around 289.0 eV, ambiguously assigned to the COOH group could be fitted to create the best possible fit (signals for C═O and COOH could be separated). In the present study however, the C in the carboxyl-group is considered with one assignment at 288.0–288.6 eV, resulting in accurate fits. In the N1s spectrum, two states of the amino group can be observed: the protonated NH_3^+ amino group at 401.5 eV dominates the spectrum while the deprotonated NH_2 group at 399.7 eV only shows a small contribution. In the O1s spectra, three peaks can be determined. The dominating low-BE component observed at 531.2 eV is assigned to the keto-oxygens of deprotonated carboxyl groups, while the protonated carboxyl-group is assigned to contributions at 532.7 eV. In the case of a deprotonated carboxyl group, both oxygen atoms contribute to the signal at this binding energy and the electrons can be considered as delocalized between them, causing a shift to lower BEs. In contrast, the BEs for the protonated carboxyl-group, due to the present hydroxyl oxygens, are shifted to higher values.[45] In addition, the protonated COOH group has two separate chemical environments for oxygen O═C–OH occurring at lower BE and O═C–OH at higher BE with a 1 to 1.5 eV BE shift between them.[56] However, like in most of the literature, this double assignment and therefore, addition of another peak was not performed in this study. The differentiation between protonated and deprotonated carboxyl groups was sufficient for this study. The third contribution in the O1s spectrum of alanine at 534.4 eV was assigned to residual water attached to the surface or in the upper layers of the sample, probably crystal water. This assignment was based on literature

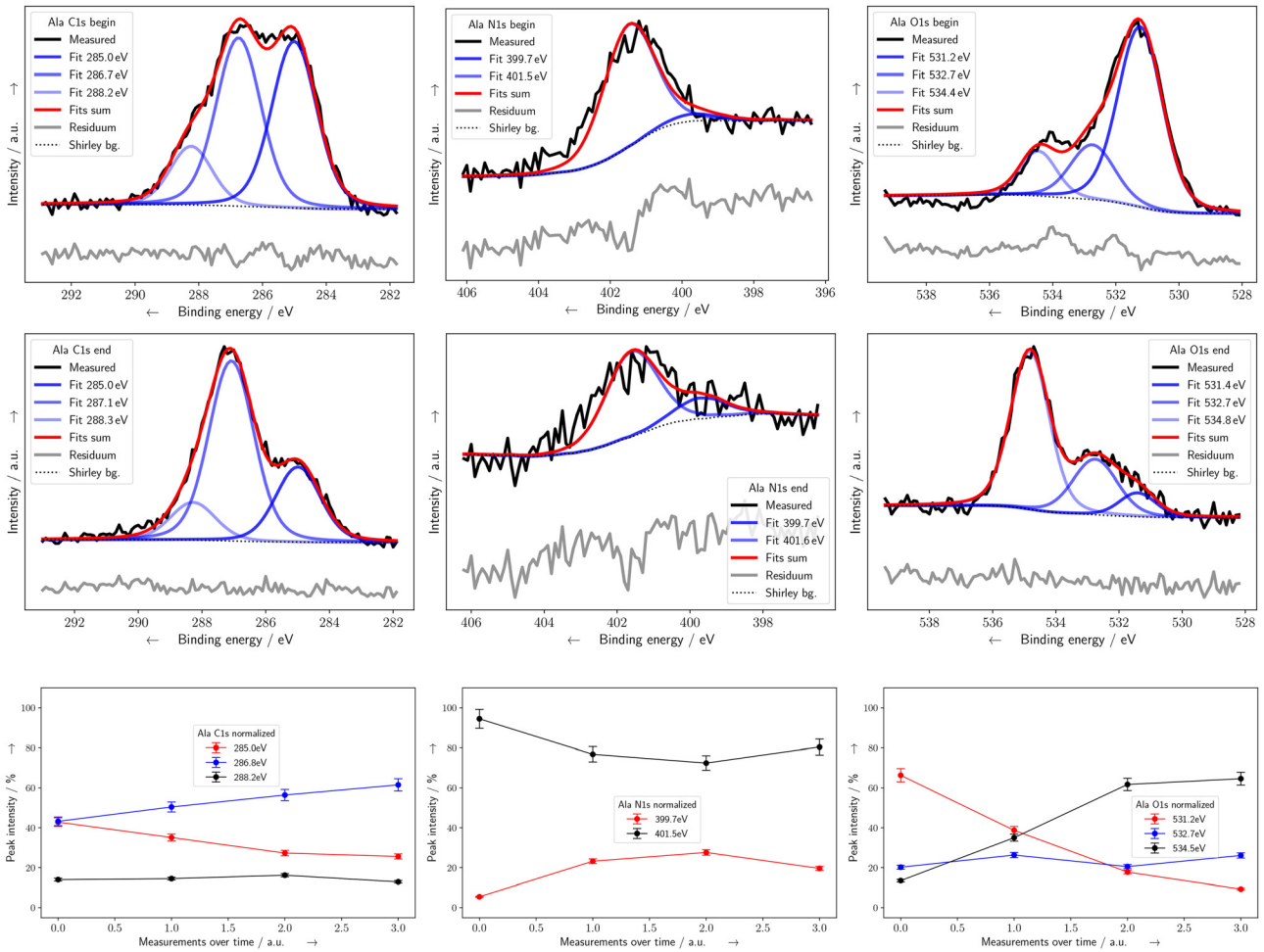

Fig. 3 XPS spectra and according time dependent normalized peak areas of XPS signals of alanine under UHV conditions. C1s (left column), N1s (center column) and O1s (right column) spectra are shown for the beginning (top row) and end (center row) of the exposure. In addition, Voigt peak fits (blue), the sum (red), the Shirley background (black dotted) and fitting residuals (grey, shifted to lower *y* values) are shown. Intensities and fitting details can be found in the SI. Time-dependent normalized peak areas are shown in the bottom row. Binding energies were adjusted with respect to C1s at 285.0 eV. The percentage of the intensity is given with respect to the total integrated peak area at the beginning of the irradiation. Assignments are according to Table 1. Error bars were determined using a matrix inversion approach. Lines are guides to the eye.

values for liquid water under UHV conditions.[57] The number of peaks and their respective areal contributions correspond to the known structural features of alanine with a simple CH_3 side-chain, with the addition of a small contribution from residual crystal water. It can be stated that the zwitterionic state of alanine is dominant at the beginning of the irradiation since protonated NH_3^+ and deprotonated COO^- dominate their spectra, visible in N1s and O1s spectra, respectively. This was expected, since this zwitterionic status is the most stable form of amino acids in solid form. These results are in line with other studies of alanine, where condensed samples were investigated.[45,47,55]

In the end of the X-ray exposure of alanine several changes in the spectra can be observed (Fig. 3 centre row). Generally, changes in the peak intensities during the course of the irradiation occur due to damage at the bonds: a decrease of a relative peak occurs due to cleavage of bonds as well as detachment of the corresponding subunits or fragments from the sample surface.[3] An increase of a certain peak can be assigned to increased relative abundances of the respective bonds or to a formation of radicals, which can be precursors of new (final and stable) products, which would appear as new peaks or a clear imbalance in the residuum (grey signal in the spectra). For better overview, the time-dependent normalized peak intensities are displayed for the spectral contribution in separate diagrams (Fig. 3 bottom row). For alanine, a clear redistribution of intensities between spectral features of C1s, N1s and O1s spectra can be detected over time. At C1s energies, the relative contributions of the C–C bond at 285.0 eV decreased in comparison to the contributions of C–N and C–O at 287.1 eV and the C of the carboxyl-group at 288.3 eV, respectively. The BEs assigned to the C–N/C–O groups shift slightly from 286.7 eV to 287.1 eV over the course of the irradiation, which may indicate a radiation induced change in the electron configuration within the probed molecule or be caused by a changed charge compensation. The overall strong

change of the relative contribution of the C–C bond could be attributed to a demethylation, a C–C bond scission at the alpha C atom, where the CH_3 group of the side-chain is released from the molecule. Abdoul-Carime, Cecchini and Sanche proposed this alteration of alanine induced by low-energy electrons.[55] In the N1s spectrum, the relative contribution of the deprotonated NH_2 group at 399.7 eV increased slightly in comparison to the protonated NH_3^+ group at 401.6 eV. The relative peak areas at N1s energies show a strong decrease (see the SI Table S1), however that decrease is not visible in the time-dependent normalized peak area diagram in Fig. 3 due to the nature of the normalization (compare the analysis of XPS data section in the materials and methods section). This indicates that there is a slight shift from charged amino groups to neutral deprotonated amino groups and a deamination (C–N bond scission) of the molecule upon XPS irradiation, that was also proposed by Zubavichus *et al.*[45] Here, a simple dehydrogenation of the protonated amino group could explain the changes in the N1s spectrum, however also other more complex processes could be involved (see below). In the O1s spectrum, a similar tendency can be seen, where the relative contributions of the deprotonated charged carboxyl group at 531.4 eV strongly decreased in comparison to the neutral protonated carboxyl-group at 532.7 eV. Thus, the O1s spectra also show a tendency from charged to neutral groups, like the N1s spectra. This could indicate a proton transfer from the amino group to the carboxyl group,[58] but also other more complex processes could be involved.[45] Also the relative peak areas at O1s energies show a strong decrease in comparison to that of carbon indicating an additional decarboxylation of the molecule.[58] The contribution assigned to (crystal) water at 534.8 eV increased. The origin of the water will be discussed later, however it has to be stated that one possible origin is the formation of new peptide bonds.[45,52,59] There, two amino acids are combined to form a dipeptide, producing a molecule of water: the carboxyl-group of one amino acid (R_1) reacts with the amino-group of the other amino acid (R_2) as shown in the following formula: R_1–COO^- + NH_3^-–R_2 + radiation → R_1–CONH–R_2 + H_2O. The time-dependent normalized peak areas of all amino acids under UHV conditions are shown in Fig. 4. The O1s and N1s spectra confirm that the zwitterionic state was predominantly found in the pristine amino acids. The only exception to this is arginine, where in the N1s spectrum, the guanidine group in the side-chain (see the structure in Fig. 1) with its three neighbouring N atoms around a central C has a delocalized positive charge. Here, the amino group is in equilibrium between the protonated and deprotonated status, while in the O1s spectrum a deprotonated COO^- can be detected. This is in line with results from other studies.[23,60] In C1s BEs, the central C group from the guanidine group in the side chain is shifted to higher BEs[49] at 289.3 eV, resulting in an additional peak.

Upon prolonged exposure to X-rays, changes both in the XPS line shape and peak composition were observed for all amino acids. Principally, a tendency from zwitterionic molecules towards neutral molecules in the dry state is detectable. This effect is more pronounced in arginine than in alanine. In the time-dependent normalized peak areas of N1s, stronger decreases in the protonated amino group and respective increases in the deprotonated amino group can be detected for the other amino acids. Therefore, fragmentations at the different subunits, like decarboxylations and deaminations are proposed for all amino acids. In addition, the contributions assigned to (crystal) water increased for all amino acids except for tyrosine. This indicates complex multi-bond breakages forming H_2O as a product of radiation damage. Especially for glycine and cysteine, a formation of new peptide bonds is proposed, based on the shape of the residuum at the end of the irradiation in the N1s and O1s spectra and the contributions of peptide bonds visible in the C1s spectra. For tyrosine, however, it was not possible to obtain N1s spectra with sufficiently high SNR, neither under UHV nor NAP conditions. This is mostly due to the low relative amount of N-atoms in the molecule (see the structure in Fig. 1). For tyrosine, the elemental composition is very different from those of the other amino acids since the side-chain consists of an aromatic C-ring (phenol). This changes the C1s spectral features, leading to an additional contribution around 283.6 eV from the ring structure involving C=C bonds and further contributions from C–C bonds. These C–C and C=C are in constant equilibrium (mesomeric stabilized). Upon irradiation, a decrease in C–C peak areas in combination with a relative increase of C=C peak areas suggests relevant radiation damage in the ring structure. A ring cleavage can be suggested[54] which interrupts the mesomeric-stabilized ring structure and thus opens the further radiation-assisted conversion of single to double-bonds. In addition, a decarboxylation and further damage reactions at the amino and carboxyl groups are proposed. For cysteine, the relative amount of sulphur in comparison to carbon strongly decreases suggesting C–S bond cleavage. Therefore, in addition to the other radiation-induced damage at amino and carboxyl groups, a desulphuration is proposed.

3.1.2 Peptides. Due to the primary structure of the peptides, the chemical bonds are the same as in the pure amino acids, with the exception of the groups at the peptide backbone, which take part in the formation of the peptide bond. For the alanine penta-peptide, the addition of the peptide bond is clearly visible in all high-resolution spectra (C1s, N1s and O1s) in Fig. 5: the peptide (or amide) bonds between the single amino acid residues result in increased contributions at 288.2 eV from O=C–N in the C 1s spectrum in comparison to single amino acids. Additional peaks at 400.0 eV in N 1s and 531.8 eV in O1s are assigned to the O=C–N bond. Generally, the C–C contribution clearly dominated the C1s spectrum at 285.0 eV. In the N1s and O1s spectra, the peak assigned to the peptide bond dominates the spectra, while the N-terminal and C-terminal end groups still reflect the predominance of charged groups (NH_3^+ in N1s and COO^- in O1s spectra, respectively). For O1s energies, once more, molecular water was assigned to the peak at 534.8 eV. Besides that, it was necessary to fit an additional Auger peak at 536.5 eV. The Auger peak was assigned to a Na KLL Auger peak, reflecting the presence of sodium[61] in the sample. This impurity is a production residue and can

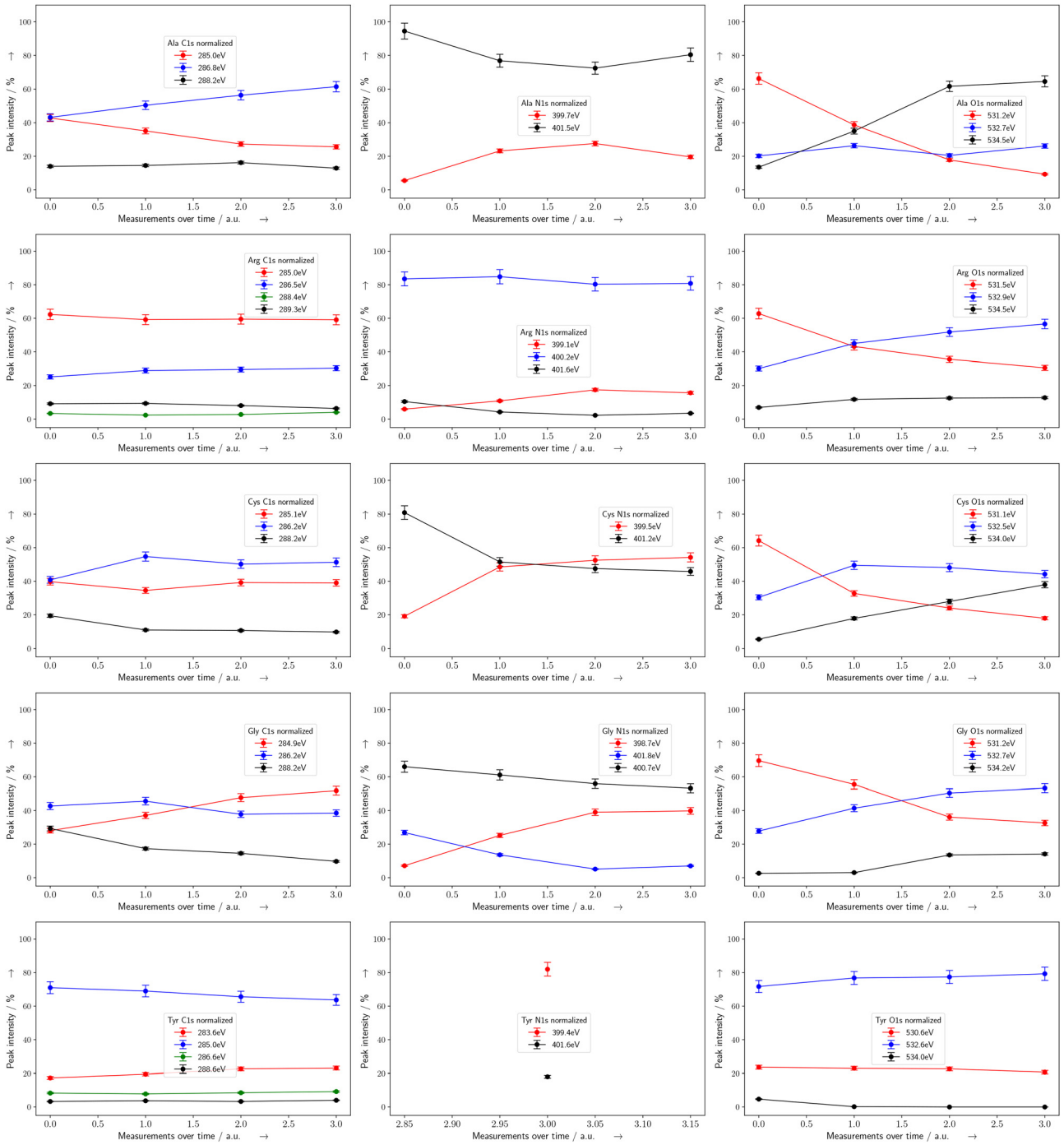

Fig. 4 Time dependent normalized peak areas of XPS signals of amino acids under UHV conditions. Evolution of XPS signals at C1s (left column), N1s (center column) and O1s (right column) binding energies are shown for alanine (Ala), arginine (Arg), cysteine (Cys), glycine (Gly) and tyrosine (Tyr). The percentage of the intensity is given with respect to the total integrated peak area at the beginning of the irradiation. Assignments are according to Table 1. Error bars were determined using a matrix inversion approach. Lines are guides to the eye.

cause an additional signal and respective overlap at O1s energies. The detection of this residual sodium (also visible in the survey spectra) reflects both the difficultly involved in purifying peptides and the sensitivity of XPS to even minor impurities. Moreover, small peptides, especially homo-peptides are very fragile and are to be handled with care. Generally, the BEs of all spectra (except 285.0 eV in C1s that was used for charge correction), are shifted to slightly lower BE as compared to the single amino acid. After irradiation, the alanine peptide shows radiation damage that differs from the damage detected at pure alanine. In C1s, N1s and O1s spectra, the relative peak areas assigned to the peptide bond decrease during the course of the irradiation. This indicates a molecular bond cleavage of the peptide bond, resulting in smaller peptide fragments and/or

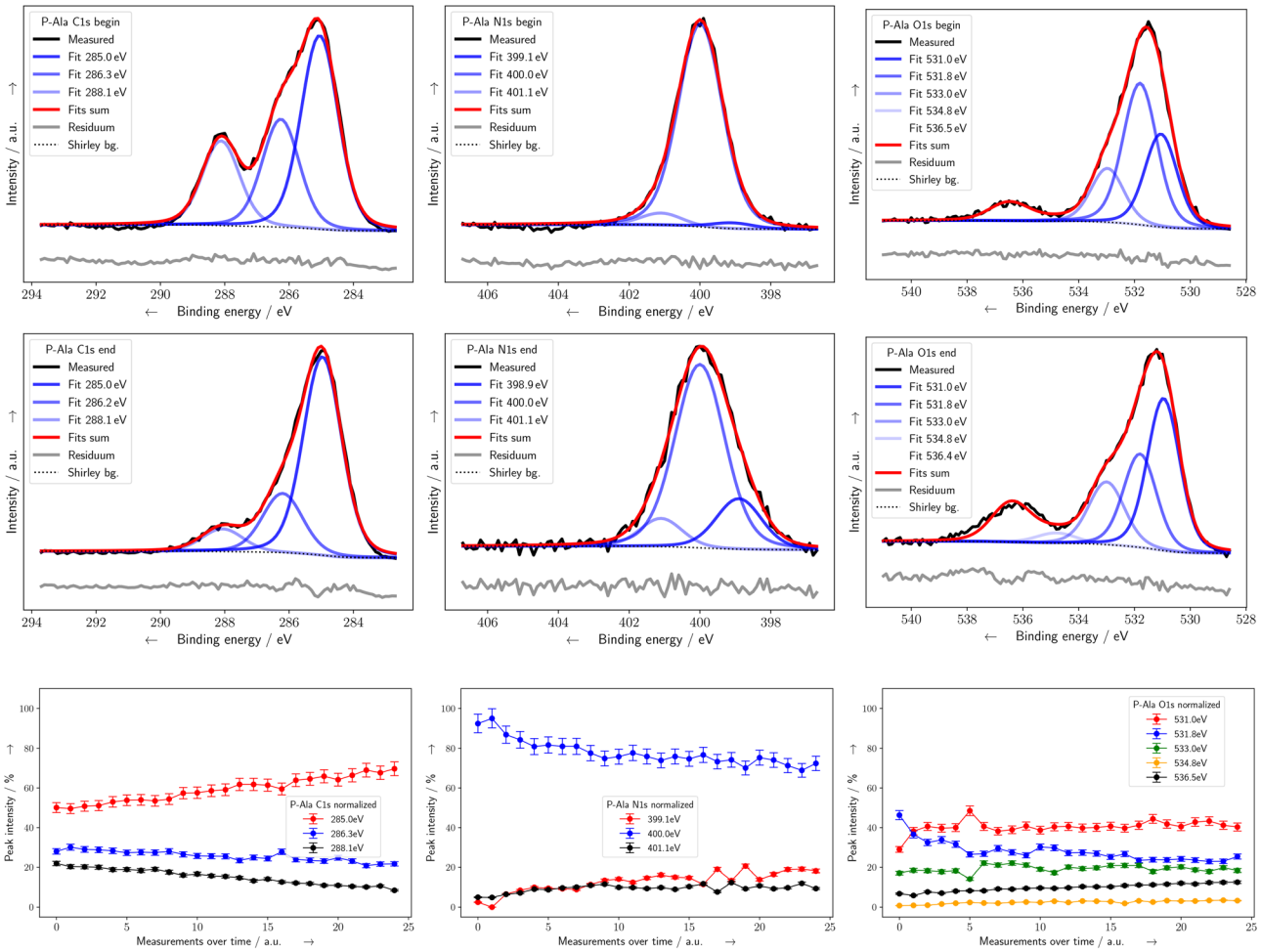

Fig. 5 XPS spectra and according time dependent normalized peak areas of XPS signals of penta-alanine (peptide) under UHV conditions. C1s (left column), N1s (center column) and O1s (right column) spectra are shown at the beginning (top row) and end (center row) of the exposure. Intensities and fitting details can be found in the SI. Time dependent normalized peak areas are shown in the bottom row. Binding energies were adjusted with respect to C1s at 285.0 eV. The percentage of the intensity is given with respect to the total integrated peak area at the beginning of the irradiation. Assignments are according to Table 1. Error bars were determined using a matrix inversion approach. Lines are guides to the eye.

single amino acids. In the N1s spectrum at the end of the irradiation, the relative contributions of NH_3^+ and NH_2 increased in comparison to the peptide bond. Here, the contribution of NH_2 groups seems more prominent than the one from NH_3^+. However, in the O1s spectrum, the contribution from deprotonated COO^- dominates the spectrum, suggesting charged end groups at the C-terminal end of the peptides. It cannot be ruled out, that new peptide bonds could be formed from the end groups of the peptides and the newly broken-off single amino acids, as once again H_2O is present at the end of the irradiation. However, no relative increase in peptide bond signals can be detected. Generally, the total amounts of nitrogen and oxygen decrease in comparison to carbon (see the SI Table S1), once again indicating a detachment from the sample surface and therefore a bond scission, like decarboxylation and deamination at the end groups. Interestingly, no relative decrease of the C–C signal in comparison to the other C1s contributions was detected like it was for pure alanine. Here, an increase of the C–C signal is detected, suggesting that the damage at the side-chain was not as fast or favoured in the peptide molecule as compared to single amino acids. This could have several reasons, including the preferential degradation of heteroatom-containing bonds. Here, bonds involving oxygen or nitrogen like the peptide bond might break faster than C–C bonds. This would reduce the relative intensity of those bonds, making the C–C signal appear relatively stronger (compare with the bottom row in Fig. 5). In addition, the peptide's linear structure and small size might allow some protection or possible rearrangement that preserves or even increases the C–C bond signature, unlike the single amino acid. The time-dependent normalized peak areas of all peptide under UHV conditions are shown in Fig. 6. Here, it can be seen that the findings for the alanine peptide also apply to the glycine peptide. The same trends can be observed with one exception in the O 1s spectrum where at the end of the irradiation the relative contributions of COO^- at 533.1 eV are more dominant than the ones from COOH. For the tyrosine peptide it was not possible to generate satisfactory fits for N 1s due to the low

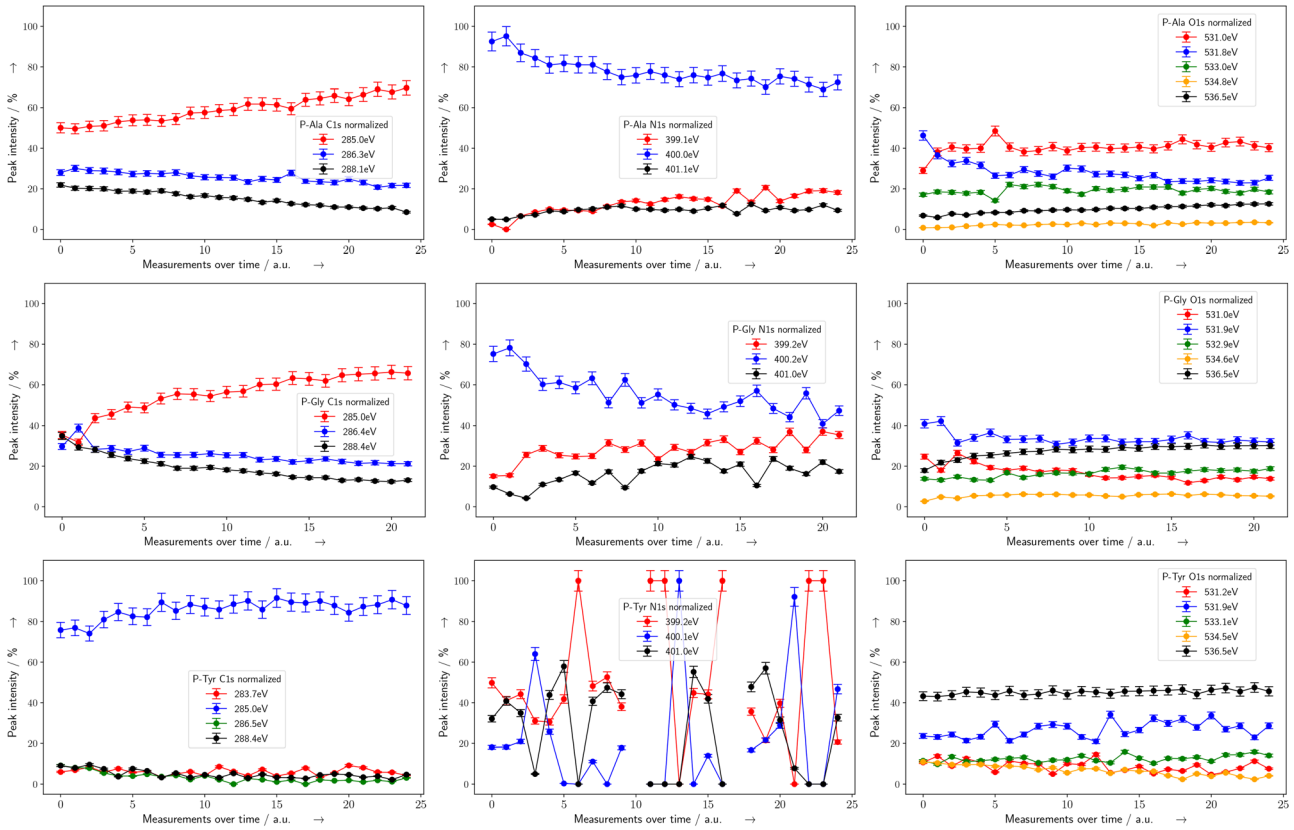

Fig. 6 Time dependent normalized peak areas of XPS signals of peptides under UHV conditions. Evolution of XPS signals at C1s (left column), N1s (center column) and O1s (right column) binding energies are shown for penta-alanine (P-Ala), penta-glycine (P-Gly) and penta-tyrosine (P-Tyr). The percentage of the intensity is given with respect to the total integrated peak area at the beginning of the irradiation. Assignments are according to Table 1. Error bars were determined using a matrix inversion approach. Lines are guides to the eye.

signal-to-noise ratio. However, the respective contributions in the C 1s and O 1s spectra and the relative peak areas suggest that there is a slight decrease for the peptide signal as well. Nevertheless, the changes are not as pronounced as with alanine and glycine peptides. This might be due to the overall different elemental composition of the tyrosine peptide or it shows that the radiation response is actually different. In the C 1s spectrum, a relative increase of the C=C signal can be seen, strongly suggesting additional damage at the aromatic ring. Here, a ring cleavage is proposed similar to the single amino acid tyrosine that was already presented above.

3.1.3 Gene-V protein. Gene-V protein consists of 87 amino acids that are connected through peptide bonds. In the XPS spectra in Fig. 7, the superposition of the signals of the single amino acids and their respective chemical bonds can be seen. There are several other additional amino acids present in G5P which were not investigated in an isolated manner in this study. This and the generally high amount of chemical bonds make the interpretation of the spectra relatively complex.

G5P shows similar spectral features as the homopeptides: in the C1s spectrum, C–C bonds at 285.0 eV, for N1s and O1s bonds the peptide bonds (at 400.1 eV and 531.8 eV respectively) dominate the spectra. In the C1s spectrum there are other contributions from C=C bonds at 283.4 eV from side-chains, from C–N, C–O and C–S at 286.5 eV and the peptide bond as well was carboxyl and keto groups at 288.1 eV. In the N1s spectrum, next to the peptide bond, the contributions from protonated (401.5 eV) and deprotonated (399.0 eV) amino groups are relatively low and similar in intensity. In the O1s spectrum, no contribution from protonated COOH could be observed, indicating that the C-terminal end group only exists in charged, deprotonated from, assigned to 530.5 eV. This was expected due to the present peptide backbone of the protein. The fit of (crystal) water was not possible here. Unfortunately, due to the low relative amount of sulphur in the whole protein molecule, a satisfactory detection of sulphur S 2p signal was not possible due to the unfavourable signal-to-noise ratio. This would have given valuable data to the development of S–S bridges within an intact protein under the influence of radiation. At the end of the irradiation, the protein shows different spectral features than before, indicating radiation damage. The peptide bond signal decreased in all spectra. However, they remain present over the course of the irradiation, suggesting a less strong decrease as compared to the peptides. In addition, in the N1s spectrum, the contribution from NH_2 groups increases strongly while in O1s the contribution from both COO^- and COOH increase. This suggests that also in the protein, radiation causes the breakage of peptide bonds,

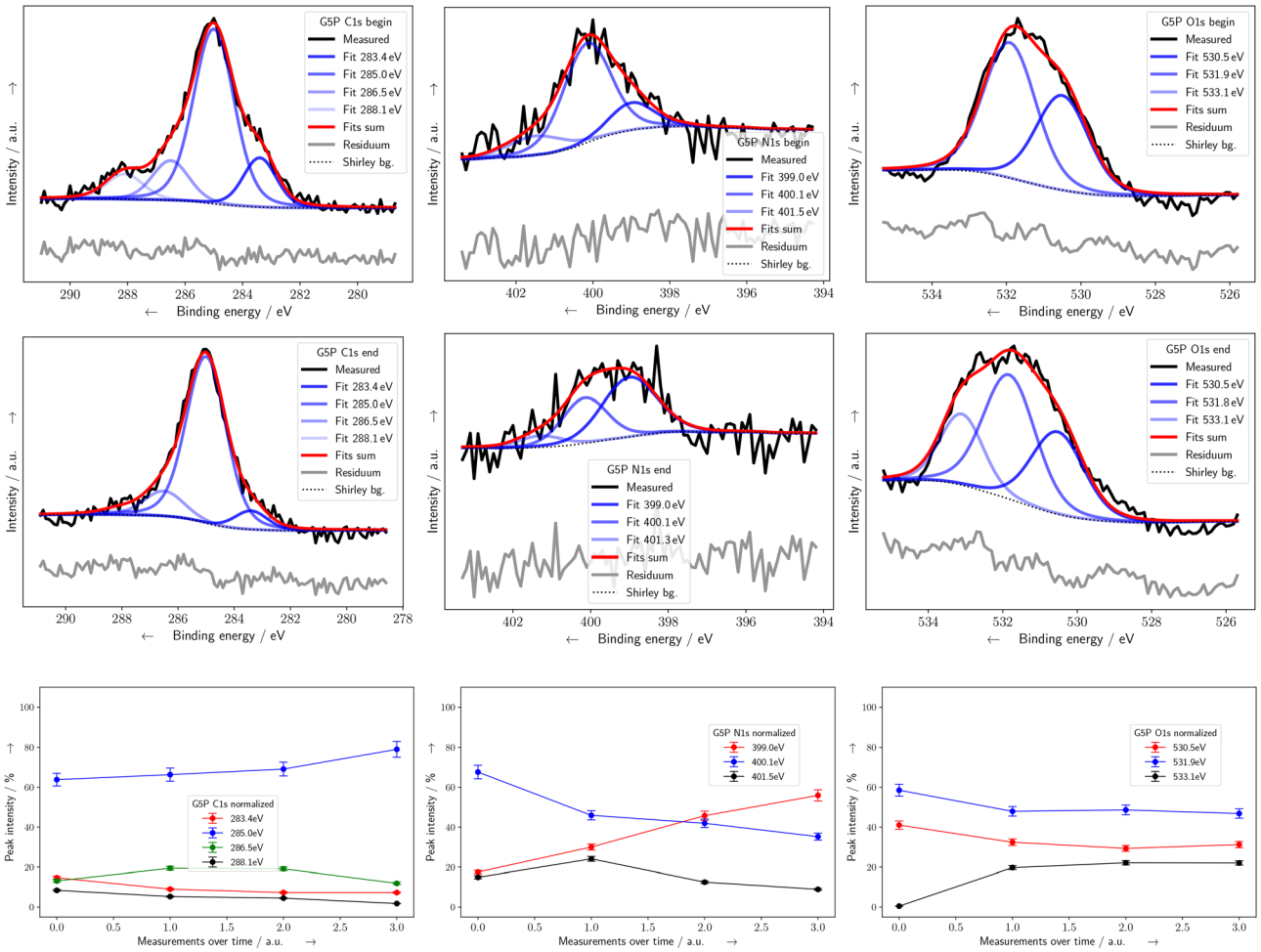

Fig. 7 XPS spectra and according time dependent normalized peak areas of XPS signals of gene-5 protein under UHV conditions. C1s (left column), N1s (center column) and O1s (right column) spectra are shown at the beginning (top row) and end (center row) of the exposure. Intensities and fitting details can be found in the SI. Time dependent normalized peak areas are shown in the bottom row. Binding energies were adjusted with respect to C1s at 285.0 eV. The percentage of the intensity is given with respect to the total integrated peak area at the beginning of the irradiation. Assignments are according to Table 1. Error bars were determined using a matrix inversion approach. Lines are guides to the eye.

leading to newly opened C- and N-terminal ends of smaller peptides. The formation of new peptide bonds could be possible but seems rather unlikely under the conditions in the dry sample, just like for the peptide samples, however it cannot be totally ruled out. In addition, a fragmentation of the end groups of the intact protein but also the new fragments is proposed since the overall relative peak areas of oxygen and nitrogen decrease. This suggests that decarboxylations, deaminations, dehydrogenations and several other more complex reactions are likely to occur in G5P as well, as was already shown for single amino acids and short peptides above. The measurements under UHV were needed to compare our set-up and the behaviour of our samples with literature values. Here the charge compensation was provided by the UHV-XPS system. In contrast, during our NAP-XPS measurement the charge compensation is achieved by the presence of gaseous water. Since the UHV and NAP measurements were performed in different devices which differ in a variety of properties (*e.g.* X-ray fluence, incident angle, spot geometry, transmission function, charge compensation) the respective results can only be compared qualitatively, as was discussed in detail in our previous work.[9]

3.2 Influence of water to radiation damage

The influence of water to radiation damage can be studied with near-ambient pressure XPS. For this method, a water atmosphere is applied above the solid sample. The pressure in the sample chamber is kept as constant as possible so that the gaseous water atmosphere above the sample also has constant properties. Under these conditions, the gas molecules have a mean free path of less than 1 μm.[9] Thus, only X-ray interactions near the surface can produce reactive species which are able to reach the probes[9] and generate relevant radiation damage. As a comparison: XPS probes the sample until a depth of about 10 nm. Regarding the spectral properties, a strong peak assigned to molecular water from the atmosphere above the sample should appear in NAP O1s spectra at about 535.0 eV. A sharp and defined peak indicates sufficient hydration of the

atmosphere at the sample surface.[57] Due to the presence of water, with NAP XPS, generally, a smaller SNR is obtained, due to the increased scattering of the photoelectrons at the gaseous water. Thus, results might be more difficult to interpret as compared to results from UHV measurements. In this NAP XPS study, single amino acids and G5P protein were probed.

3.2.1 Amino acids. In Fig. 8, the NAP XPS spectra (C1s, N1s and O1s) of alanine are displayed. In the O1s spectrum, the presence of the water atmosphere (gas phase signal) above the sample is clearly visible due to the strong, narrow peak at 535.2 eV. As expected, the O1s peak for gas phase water is noticeably narrower[38] as compared to the crystal water (liquid water) that was already described above (for example in Fig. 3, O1s spectra). Other than that, the spectral features of alanine do not differ fundamentally from the spectra from the previously described measurements under UHV conditions. In both measurements, the same peak assignments could be performed (see assignment above). From the N1s and O1s spectra from the beginning of the measurement, it can be stated that once again, a zwitterionic status of alanine is present (strong contributions from NH_3^+ at 401.4 eV and COO^- at 531.3 eV, respectively). In the end of the X-ray exposure of alanine only few changes in the spectra can be observed (Fig. 8 centre row). The time-dependent normalized peak intensities (Fig. 8 bottom row) eventually also show only minor changes. For C 1s, a slight increase in C–C peak intensity can be observed. This contrasts with the proposed demethylation under UHV conditions, where the C–C contribution clearly decreased. For N 1s a slight tendency towards more neutral NH_2 groups can be seen, however the majority of the amino groups stay in their protonated form. For O 1s, the same tendency towards more neutral groups can be detected. Here, only the total oxygen decreases in comparison to carbon, indicating that the major damage occurs at the carboxyl groups. The time-dependent normalized peak areas of all amino acids under NAP conditions are shown in Fig. 9. The O 1s and N1s spectra confirm that predominantly the zwitterionic state is found in the amino acids at the beginning of the irradiation.

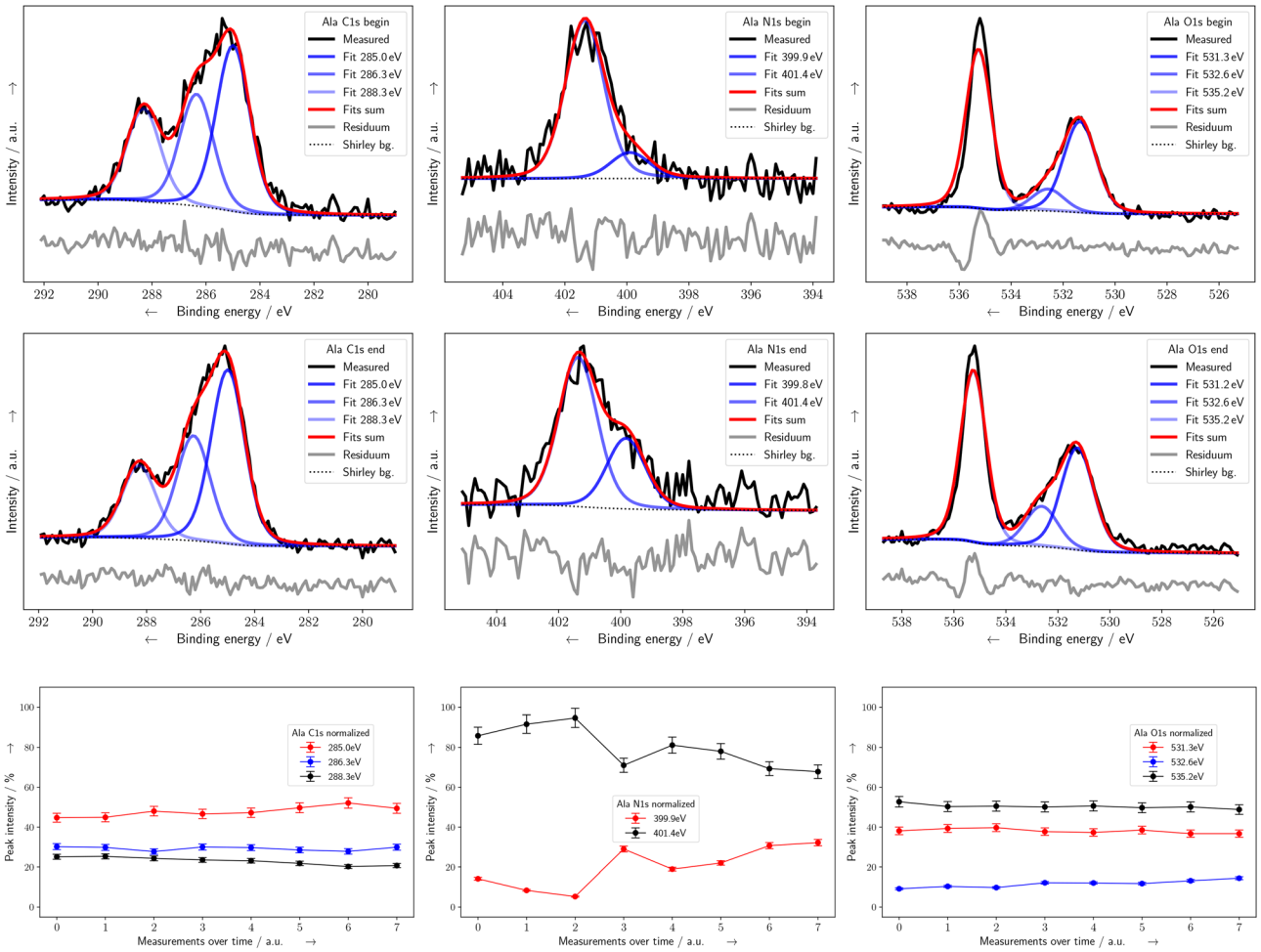

Fig. 8 XPS spectra and according time dependent normalized peak areas of XPS signals of alanine under NAP conditions. C1s (left column), N1s (center column) and O1s (right column) spectra are shown at the beginning (top row) and end (center row) of the exposure. Intensities and fitting details can be found in the SI. Time dependent normalized peak areas are shown in the bottom row. Binding energies were adjusted with respect to C1s at 285.0 eV. The percentage of the intensity is given with respect to the total integrated peak area at the beginning of the irradiation. Assignments are according to Table 1. Error bars were determined using a matrix inversion approach. Lines are guides to the eye.

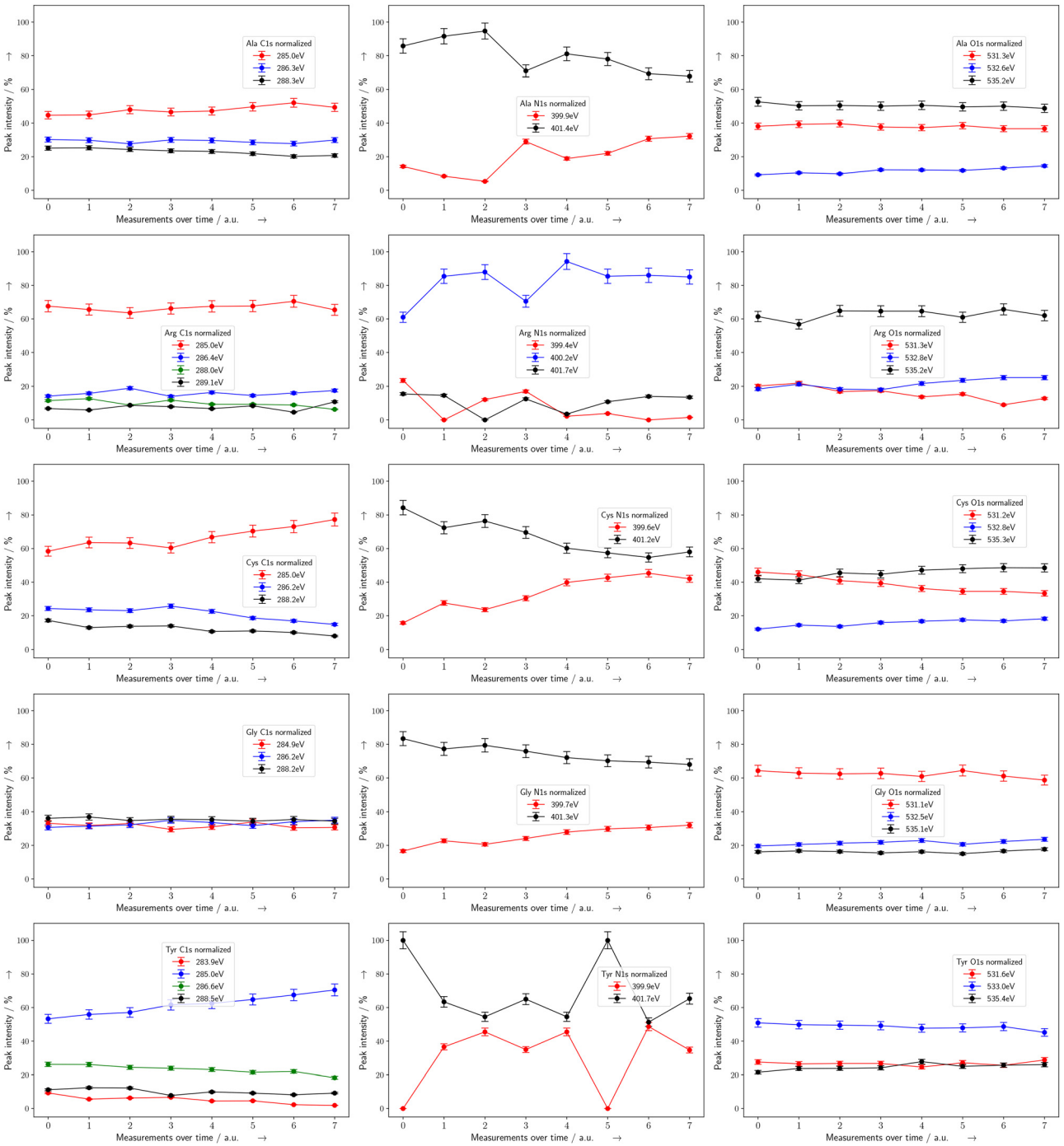

Fig. 9 Time dependent normalized peak areas of XPS signals of amino acids under NAP conditions. Evolution of XPS signals at C1s (left column), N1s (center column) and O1s (right column) binding energies are shown for alanine (Ala), arginine (Arg), cysteine (Cys), glycine (Gly) and tyrosine (Tyr). The percentage of the intensity is given with respect to the total integrated peak area at the beginning of the irradiation. Assignments are according to Table 1. Error bars were determined using a matrix inversion approach. Lines are guides to the eye.

The only exception to this is once again arginine, where in the N 1s spectrum, the guanidine group in the side-chain has a delocalized positive charge.[23,60] Here, the amino group has a balance between the protonated and deprotonated states, just as in the O 1s spectrum where the protonated and deprotonated carboxyl-group show about the same contribution. Upon prolonged exposure to X-rays, slight changes both in the XPS line shape and surface composition were observed for all amino acids. A tendency from zwitterionic molecules towards more neutral molecules under the influence of the water atmosphere is detectable for glycine and cysteine. This effect is more pronounced than for alanine. In the respective time-dependent normalized peak areas of N1s, stronger decreases in the protonated amino group and respective

increases in the deprotonated amino group can be detected. However, the majority of the amino groups stay charged. For arginine, this shift is not visible in the N1s spectrum at the end of the exposure. Here, the contribution from neutral, deprotonated amino groups decreases to zero, while some protonated amino groups remain present, next to the guanidine group in the side-chain. A charge shift from the side-chain to the amino group could be possible, but also a double positively charged molecule (with both the amino and guanidine group carrying a positive charge). In the O1s spectra of arginine, the contribution from neutral protonated carboxyl groups is predominant compared with those of deprotonated groups. Unfortunately, the generation of satisfactory fits for N1s of tyrosine was not possible. However, in the O1s spectrum of tyrosine nearly no change in the contributions can be detected. The total nitrogen areas compared to carbon decreased for arginine and cysteine, still indicating a loss of amino groups and a possible deamination. The total oxygen areas compared to carbon decreased for arginine, cysteine, glycine and tyrosine, indicating a loss of carboxyl groups and a possible decarboxylation. In the C1s spectra, an increase of relative peak intensities of the contribution of C–C at 285.0 eV can be detected for all amino acids. The other contributions show only slight changes. For tyrosine, a decrease in contributions from C=C bonds can be seen in the C1s spectrum. This stands in contrast to the results under UHV where the C=C bonds increased relatively over time (see Fig. 6 for comparison). Here under NAP conditions and under the influence of the water atmosphere and the respective reactive particles, due to the decrease of C=C and the ratio of C=C and C–C, different radiation damage products can be expected. Here, a cleavage of the ring is not very likely. The higher contribution from C–C compared to C=C bonds probably derives from the general relative change of the total carbon amount in comparison to nitrogen and oxygen. Usually, under the presence of hydroxyl radicals and other oxidative radicals, additions of hydroxyl-groups to the ring[62] and/or the formation of tyrosine dimers through a bridge between two tyrosine rings[63] is observed. Theoretically, the addition of another hydroxyl-group would cause an increase of the relative contribution assigned to OH located at the ring at 533.0 eV in the O1s spectra. However, here no increase can be detected. Actually, no change in the relative contributions of the signal at 533.0 eV can be detected. In the case of tyrosine dimerization, a multitude of possible products through the formation of various bridges are theoretically possible, which have already been characterized by Gatin *et al.*[63] They observed, for example an *ortho–ortho* dimerization. In iso-dimerization, an O-bridge would be formed between the two rings, which could lead to an enlargement of the mesomeric-stabilized system (from one ring to two rings). Since we did not observe additional contributions in the O1s spectra upon irradiation, such as those resulting from the additional C–O–C bridge in iso-dimerization, this type of dimerization is not likely under the present conditions. However, *ortho–ortho* dimerization would not produce any new, detectable bonds (since the newly formed bridge would belong to the mesomeric-stabilized system) and is therefore difficult to detect *via* XPS. Thus, in this study it cannot be confirmed that either of the two mentioned processes of OH-addition to the tyrosine ring or dimerization of tyrosine occur.

For cysteine, the relative amount of sulphur in comparison to carbon decreases suggesting C–S bond cleavage also under NAP conditions.[64] Therefore, in addition to the other radiation-induced damage at amino- and carboxyl-groups, a desulphuration is once again proposed. Principally, the formation of peptide bonds between the single amino acids cannot be ruled out. However, under NAP conditions, the formation of molecular water in the reaction process is hard to detect due to the water already present in the sample chamber. There, the inherent presence of water makes any fluctuations or the addition of molecular water from reactions of the sample difficult to detect during the course of the measurement. In addition, the overall lower SNR ratio and thus the respective residuum of the fits command a cautious interpretation of the fits. Principally, the decrease in damage upon hydration is surprising, since a strong increase in radiation damage from indirect damage by the additional presence of radical species and related damaging channels was expected, similar to previous studies performed on DNA.[9] This was due to the presence of water that, through radiation-induced radiolysis, produces various reactive species. These species from NAP measurements were expected to cause more severe damage to the samples than under UHV conditions. This behaviour will be discussed in detail further below.

3.2.2 Gene-V protein. In Fig. 10 the spectra and time-dependent normalized peak areas for gene-V protein under NAP conditions are shown. Here, the spectra at the beginning of the irradiation (top row) show contributions and line shapes similar to the spectra recorded under UHV conditions (compare with Fig. 7), with the exception of a clearly defined water peak at 535.3 eV. In the C1s spectrum, the C–C bonds at 285.0 eV and for the N1s and O1s BEs the peptide bonds (at 400.2 eV and 532.6 eV, respectively) dominate the spectra. In the C1s spectrum there are other contributions from C=C bonds at 284.5 eV from side-chains, from C–N, C–O and C–S at 286.4 eV and the peptide bond as well was carboxyl and keto groups at 288.1 eV. In the N1s spectrum, the SNR unfortunately does not allow for a clear identification of contributions. In the O1s spectrum, contributions from both protonated and deprotonated carboxyl groups were detected next to the peptide bond. This indicated that the C-terminal end group of the protein exists in both protonated and deprotonated forms. Unfortunately, due to the low proportion of sulphur in the whole protein molecule, a satisfactory detection of sulphur was not possible. At the end of the irradiation (Fig. 10 center row), the protein shows no clear difference in spectral features than before. The peptide bond signal in C1s and O1s spectra does not show significant changes. The peptide bonds remain present throughout the course of the irradiation, suggesting a less strong influence of radiation damage on the peptide backbone of the protein. A breakage of peptide bonds as proposed for G5P under UHV conditions, cannot be detected under a water

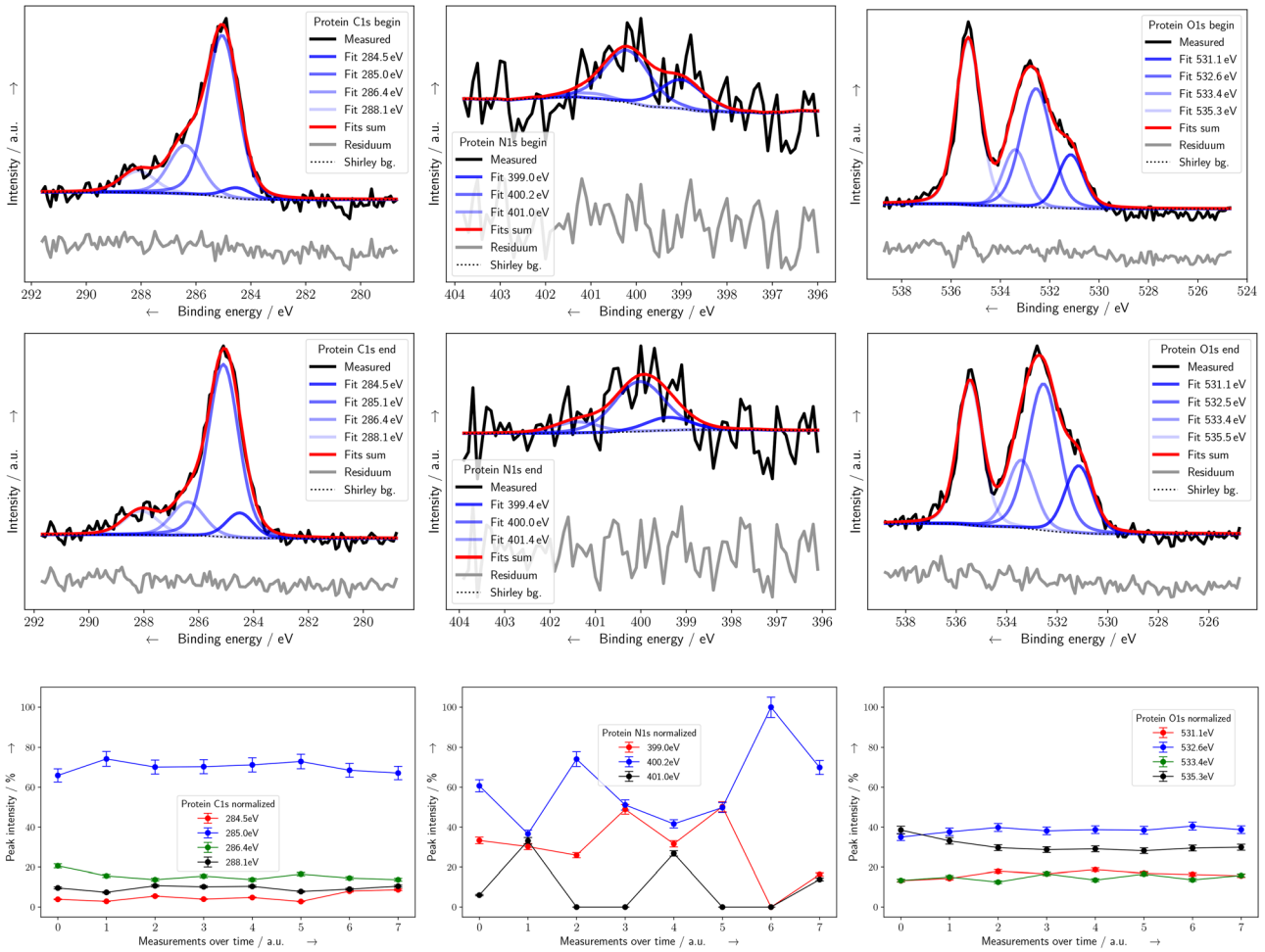

Fig. 10 XPS spectra and according time dependent normalized peak areas of XPS signals of gene-5 protein under NAP conditions. C1s (left column), N1s (center column) and O1s (right column) spectra are shown for the beginning (top row) and end (center row) of the exposure. Binding energies were adjusted with respect to C1s at 285.0 eV. Intensities and fitting details can be found in the SI. Time dependent normalized peak areas are shown in the bottom row. The percentage of the intensity is given with respect to the total integrated peak area at the beginning of the irradiation. Assignments are according to Table 1. Error bars were determined using a matrix inversion approach. Lines are guides to the eye.

atmosphere within the given data, indicating a decreased susceptibility for radiation attack of the peptide backbone in the presence of water. This will be discussed further below in the context of varying reaction rates of damaging agents independent of the local environment.

Furthermore, unlike in pure amino acids, no increase in the contribution of C–C bonds at 285.0 eV was detected here. This indicates less relative fragmentation of nitrogen or oxygen containing groups in the side chains, as well as N- and C-terminal sides of the protein. The same holds for the direct comparison of protein degradation between UHV and NAP conditions – showing an increased stability of the protein in the presence of water.

4 Discussion

The radiation response of amino acids, small peptides and a protein were investigated under ultra-high vacuum and near-ambient pressure conditions. Generally, when water is present, amino acids are in a permanent equilibrium between the zwitterionic and neutral configuration through an intermolecular proton transfer. The environment of the molecules can favour one form or the other whereby the present configuration could benefit certain damage pathways: the electron configuration and thus the occupancy of the orbitals in zwitterionic and neutral forms differ. Sanche *et al.* observed the alteration of condensed films of amino acids under vacuum conditions induced by low-energy electrons. They stated that a zwitterionic amino acid requires less energetic effort to dissociate[55] and is therefore more vulnerable to radiation attacks. A zwitterionic state was proposed for all amino acids and peptides (except arginine that was already described above) from the N1s and O1s spectral features at the beginning of the irradiations. This is expected and was already stated in the literature for condensed samples.[45,47,55] Induced by X-ray radiation, a tendency from zwitterionic molecules towards more neutral molecules was found for both UHV and NAP conditions

in this study. A deprotonation of the initially protonated amino group could occur though inter- or intramolecular proton transfer, converting the zwitterion into a neutral molecule. When Tzvetkov *et al.* analyzed glycine thin-films under XPS conditions, they compared the rates of deprotonation of NH_3^+ with the rates for protonation of COO^-. In theory the rates should be equal to each other if an intramolecular proton transfer occurs. In practice, however, the rates were not comparable indicating that the increasing NH_2-to-NH_3^+ ratio cannot be associated with the transition from zwitterionic to neutral molecules. They concluded that the transition presumably takes place during prolonged irradiation but is not the main irradiation effect.[52] Bozack *et al.* assigned the decrease of NH_3^+ to a core ionization of the protonated N-atom.[58] They investigated radiation-induced changes in lysine powders during XPS experiments and also stated a zwitterion to neutral molecule transition and a decarboxylation of the amino acid. Zubavichus *et al.* also documented amino-group deprotonation of amino acids, suggesting that this is most likely not a zwitterion to neutral molecule transition, but rather a formation of CN multiple bonds.[45] In this study, the formation of multiple-bonds, involving carbon double- or triple-bonds (except C═C for tyrosine and the protein) as well as nitrogen-bonds, were not fitted into the spectra. However, the formation of potential new bonds can be observed by the appearance of additional peaks (the altered signal shape and large spikes) in the residuum in the spectra (gray line) under the given fitting conditions.

In this study, radiation damage was detected for all samples and under both UHV and NAP conditions. The damage generated in vacuum can be attributed to direct effects originating from X-ray photons or secondary electrons, since water is mostly absent under UHV conditions. For the amino acids, the contribution assigned to (crystal) water (for example for alanine at 534.8 eV) increased over time. A step-wise formation can be proposed, based on the slowly increasing peak intensity of the respective peak displayed in the diagrams for time-dependent normalized peak areas (Fig. 3, bottom row for alanine). The molecular water could be a product of diffusion of crystal water from deeper layers of the sample during irradiation, possibly migrating to the surface by local heating effects, which then resides temporarily on the sample surface. Also, thermally activated dehydration of carboxylic acids and amino acids is known.[65] However, since the contribution is so significant and such a quantity of water is highly unlikely in a dried sample – especially under vacuum conditions – the origin of the water must be sought in radiation-induced processes. This different origin and therefore chemical surrounding of the water could contribute to the shifted BE (from 534.4 eV at the beginning to 534.8 eV at the end of the exposure). One possible origin of the water is a dehydroxylation (C–OH – bond scission) at the carboxyl group and the dehydrogenation at another subgroup, forming H_2O in the process. But also a decarboxylation followed by cross reactions with neighbouring amino acids could be possible. A recombination of bonds due to reduced mobility of decomposition products in the condensed samples should not be neglected. Generally, a decomposition of the carboxyl-groups into CO_2 and H_2O in a free radical process is likely under the conditions and was already described.[45] Another well-known biological process that produces water and involves amino acids is the formation of new peptide bonds: two zwitterionic amino acids form a new peptide, by subtraction of one O-atom from a carboxyl-group and two H-atoms from the other molecules protonated amino group, resulting in one water molecule and a dipeptide, respectively.[45,52,59] This process could be proven though the fitting of additional peaks at around 400.0 eV for N1s BEs and 532.0 eV for O1s BE for the newly formed O═C–N peptide bond (as performed in Fig. 5 for the alanine peptide) since the peptide formation leads to the presence of amide oxygen centers. The contribution of C 1s BEs would result in increased contributions at 287.1 eV for C–N and 288.3 eV for O═C–N, respectively. Without these additional peak fits, only the residues (grey lines) of the spectra could show the formation of such a peptide bond by a strong deflection and thus indicate a missing bond within the fits. For alanine, resulting peptide bonds are unlikely since no clear deflections can be detected within the residues of the N1s or O1s spectra of the end of the irradiation. However, other amino acids like cysteine and glycine show them, arguably indicating the formation of new peptide bonds which was already described in the literature.[45,52,59] Moewes *et al.* studied the X-ray induced decomposition of glycine powders by NEXAFS. Their results suggest that removal of an oxygen ion from the carboxyl-group induces the formation of peptides in the sample.[59] Theoretically, the presence of water in the vicinity of the samples under UHV conditions could trigger processes mediated by reactive species from water radiolysis. However, it is more likely that the water molecules present are quickly removed in the vacuum, and that no hydration shell forms under UHV conditions. Comparing the respective contributions of H_2O in O 1s spectra under UHV and NAP, the water peak profile in NAP is significantly different, namely sharper and more defined than in UHV. In addition, the water molecules present per amino acid or peptide are lower under UHV conditions as under NAP conditions, as determined from the O1s spectral intensities.

Generally, the formation of new bonds upon irradiation, like the formation of peptide bonds between amino acids or the formation of bridges between tyrosine rings, requires the spatial proximity of the molecules and the respective end groups in the solid samples, or at least a highly crowded environment as found within the nucleus of a cell.

Under UHV conditions, fragmentation processes dominated the overall damage profile leading to the dissociative desorption of radiation-induced fragmentation products from the sample surface. Several competing routes of decomposition were detected, mainly decarboxylation and deamination as well as fragmentations of the side chain like demethylation (for alanine) and desulphuration (for cysteine). One of them, the deamination of amino acids due to C–N bond scission was stated to be the major process creating amino moieties during X-ray irradiation.[52] In the O1s spectra of amino acids, a strong decrease of oxygen relative to that of carbon was detected.

This is mainly due to decarboxylation.[23,45,52,58] A chemical disintegration or fragmentation of the probed molecules as described above involves a series of (free-radical) reactions.[1,54,55,64] Besides, secondary reactions can occur inter- or/and intramolecularly, initiated by resulting free radicals.[9,45] For the irradiation with X-rays, ionization is the first step of radiation damage. Under the conditions in this study, a core-level ionization of the probed molecules is the principal ionization channel for direct damage. Here, upon ionization, an electron is ejected while the resulting electron hole can migrate within the whole molecule. This hole could lead to direct fragmentation or localize at the side chains with low electron affinity. These radical reactions can lead to deprotonation of alpha-C (cannot be directly detected with XPS but was described in the literature[45]), as well as the formation of decarboxylation and deamination products. Furthermore, the initial distribution of direct ionization events at the probed molecules correlates with the electron density at the subgroups.[66] Thus, especially the sulphur-containing side-chains of cysteine are vulnerable to direct radiation attacks. This subsequently causes the electronic restructuring and thus, the final cleavage of the C–S – bond.[64]

It is likely that more complex reactions are involved in the radiation damage of the protein as compared to single amino acids, both under UHV and NAP conditions. This is due to the more complex structure and intermolecular interactions in a protein such as hydrogen bonds and sulphur bridges. The specific electronic configuration of the single amino acids, among other factors, suggest that within proteins, certain positions of the peptide backbone are more vulnerable to LEE attacks than others.[67] Stadtman *et al.* concluded that under the absence of oxygen, aggregation dominates the radiation damage of proteins, where the protein would be converted into aggregates with higher molecular weight[68] through *e.g.* intermolecular cross-links. The presented results under UHV conditions do not show clear signs for aggregation but rather fragmentation. The absence of oxygen might not be the only factor for the formation of cross-links and aggregations but also the status of the sample (here, condensed and non-hydrated) and the used technique. However, due to the nature of the XPS measurement in UHV and the condensed nature of the sample, some processes that could be observed in diluted solutions or even gas phase experiments may not be detectable in this particular measurement. Differences with other protein studies can be attributed to biological, chemical and technical variations: the amino acid sequence (the primary structure), hydration dependent inter- and intramolecular coupling, protein conformation but also temperature, film thickness (for films) or particle size (for powders) and the local environment *etc.* could affect the decomposition kinetics of degradation mechanisms.[52] For NAP measurements, especially differences in conformation due to additional hydrogen bonds with adsorbed water molecules have to be considered. In this context, the varying sizes of the amino acids themselves, but also the peptides and the protein have to be considered as well as the presence or absence of hydrophobic or polar side-chains and their respective orientations. These properties can be assumed to lead to a local variation of the level of hydration which may lead to an actual quite inhomogeneous distribution of the water within in the sample. This might lead to an inhomogeneous distribution of production of reactive species in the near-ambient atmosphere above the samples, as further discussed below. The variety of chemical changes upon irradiation of the protein, both at the side-chains but also the peptide backbone, suggest a major alteration of the molecules' properties. This becomes most evident from the proposed breakage of the peptide backbone. In addition, changes in the amino acid side-chains as described above, will arguably lead to changes in the conformation of the protein. This and the breakage of the peptide backbone could both result in a loss of function. Unfortunately, no clear statement can be made about the functionality of the protein based on XPS analysis. Generally, the oligomeric state of G5P could influence the extent and nature of radiation damage as well. G5P is known to form highly stable homodimers in solution. Crystallographic data[21,22] reveal a well-defined dimer interface stabilized by both electrostatic interactions and hydrophobic contacts, suggesting an increased stability and higher resistance against unfolding or fragmentation, at least initially, under X-ray exposure in comparison to a monomer. These differences may lead to subtle shifts or changes in C1s and N1s peak intensities or shapes. However, in this case no particular shift or change was detected. The qualitative damage to G5P that was detected suggests that the binding of ssDNA might not be possible any more. Especially the changed charge of arginine at the side-chains (and lysine side-chains as studied by Bozack *et al.*[58]) suggest that the needed positive charges within G5P for the interaction with the negatively charged DNA might not be sufficient. Additionally, the proposed ring cleavage of tyrosine could presumably interfere with the required interaction of the (formally) aromatic side-chain with nucleobases in DNA. In comparable studies, damages were found to be irreversible. For example, Bozack *et al.*[58] noted that the radiation damage was still present in the irradiated lysine samples, even after 24 hours post irradiation and after evacuation. The same spectral characteristics were found in the samples as immediately after irradiation.[58]

Under NAP conditions, both direct and indirect effects can be observed: the X-ray radiation causes direct effects on the amino acids and the protein. Indirect effects on the studied samples through the radiolysis of water molecules from the ambience (including OH-radicals, H-radicals, short-lived water cations H_2O^+ or pre-hydrated electrons)[2] located in the first hydration shell occur. Thus, the presence of water enables different radiation damage mechanisms as compared to UHV conditions. Under NAP conditions, usually, the production of reactive oxygen species (ROS) and the modified electron transfer (ET) channels are important factors for producing radiation damage.[9] In addition, the presence of water also modifies the outcome of multiple-step reactions involving radical sites, regardless of their origin.[69]

The exact amount of water molecules at the various parts of the different molecules cannot be resolved with the applied technique. Here, we have to consider the varying sizes of the

amino acids, peptides and the protein, and the presence/absence of hydrophobic or polar side-chains, and their respective orientations. These properties can be assumed to lead to a local variation of the level of hydration which may lead to an actual quite inhomogeneous distribution of the water within the sample. Therefore, we assume that speaking of 'one value for a hydration shell' might underestimate the complexity of the different levels of hydrations, found throughout the sample. Furthermore, the layered nature of the system provides different accessibility for the 'NAP water' which is in part countered by the 'crystal water'. The crystal water in a G5P monomer is a total of 53 water molecules, which corresponds to about 0.61 water molecules per amino acid. Therefore it can be only stated cautiously, based on previous work where radiation damage to DNA under UHV and NAP XPS conditions was studied,[9] that at 5 mbar no second layer of the hydration shell is formed. Thus, the relative amount of water is lower than in a cellular environment. Hence, the present experiments are expected to have a relatively higher contribution from processes involving quasi-direct effects from for example H_2O^+ than from hydroxyl radicals, which are produced in higher quantity in bulk water.

Radiation damage was detected under NAP conditions. However, an increase in damage, compared to UHV conditions, was not detected with the used NAP-XPS set-up. This is unexpected, since the very same set-up delivered high-quality spectral data of DNA and revealed an overall increase and change of the type of DNA damage under NAP conditions.[9] There, it was also proven by particle scattering simulations and comparison of measurements under a N_2 and H_2O atmosphere, that the stated change in radiation damage under the different atmospheric conditions was not caused by direct effects, but is related to the presence of water. The complexity of DNA is comparable to the complexity of a protein, so that satisfactory results, just like for DNA, were expected. Under NAP conditions, water molecules are present above the sample surface. Usually, only ionizing events in the vicinity (about up to 7–8 nm) of the target lead to relevant indirect effects to the target (like in the first and second hydration shell).[2] However, water radiolysis and thus the production of secondary electrons and free radicals is considered to happen randomly along the radiation path in the sample chamber during NAP XPS.[9] Here, both the water and the present samples (amino acids or protein) allow energy transfer between neighbouring molecules. One efficient intermolecular relaxation process which depends strongly on the environment is intermolecular coulombic decay (ICD).[70] For example, Richter *et al.* irradiated cluster ensembles of 5–246 water molecules with photons to investigate the competition between proton transfer and ICD in water.[71] They found that the efficiency of the ICD for small water clusters is surprisingly low and that the proton transfer between two neighbouring water molecules plays a crucial role in radiation chemistry upon ionization of water. They state that after proton transfer in water, instead of a highly damaging slow electron (that would result from ICD[70]), a hydrogen atom of relatively low potential for biological damage appears. They conclude that small systems that are strongly hydrogen-bonded are less vulnerable to damage from slow auto-ionization after irradiation than previously thought.[71] This could be one possible explanation for the observed reduced (bio-)radiation damage under a NAP atmosphere, since the conditions named by Richter *et al.* apply here: a small (water) system is observed and the investigated amino acids and the protein itself obtain (strong) hydrogen bonds. A change in the charge transfer and therefore a modification of the indirect damage can be proposed. However, in the present NAP set-up the water is expected to behave differently than a gas phase water cluster, since here a hydration layer is formed above the amino acids and the protein. The ambient water and the biological samples are expected to influence each other and possibly change the reaction rates of reactive species.

Early studies on reaction rates of (hydrated) electrons with amino acids were performed by Braams[72] where amino acids were treated with electron pulses in aqueous solution and the respective absorption was followed by an oscilloscope. There, it was stated that some amino acids are more reactive with hydrated electrons than others:[72] cysteine and histidine show high reaction rates of 10^9 to 10^{10} M^{-1} s^{-1} at pH 6.1–6.3 with hydrated electrons and are therefore more vulnerable to attack by electrons as compared to glycine and alanine with respective reaction rates of $\approx 10^6$ M^{-1} s^{-1} at pH 6.4–6.8, for example.[72] This sensitivity of cysteine, especially the sensitivity in the S-containing side-chain was also observed in this study. In addition, cysteine residues were also determined to be highly reactive with OH-radicals, where reaction rates were determined to be in a range of 2.4×10^9 (ref. 73) to 1.9×10^{10} (ref. 74) M^{-1} s^{-1} by others. However, in the local environment of a protein, the accessibility and reactivity of cysteine residues can be important factors and the shown effective reaction rates are likely to differ. Generally, the reaction rates of OH-radicals with amino acids depend on the amino acids chemical form (zwitterion, neutral, cation, anion), the type of amino acid and the specific reaction conditions such as temperature and pH: Masuda *et al.* studied the reaction rates of OH-radicals with amino acids and enzymes in water after irradiation with a gamma source.[75] They found that the reaction rates of OH-radicals with different amino acids vary drastically: here, high reactivity of OH-radicals with amino acids with aromatic rings (like tyrosine) was determined, while other amino acids only show low reaction rates.[75] In this study, no clear evidence for the addition of the OH-group to the aromatic ring of tyrosine was found, which was surprising, as already discussed above. For alanine, the measured second order reaction rate constants with OH-radicals at 298 K and pH 6.0 are $\approx 6.8 \times 10^7$ M^{-1} s^{-1} while for glycine the value is drastically lower at $\approx 1.5 \times 10^7$ M^{-1} s^{-1},[76] showcasing the importance of the chemical structure involved. In a protein, that consists of numerous amino acids, it can be concluded that some amino acids are more vulnerable towards an OH-radical attack than others.[73,75,76]

In contrast, the reaction rate constants of OH-radicals with double-stranded DNA is in the range of 1×10^9 to 2×10^9 M^{-1} s^{-1}.[77] Generally these rates (and also the reaction rates of hydrated and low-energy electrons) depend on factors such

as DNA structure, pH and ionic conditions.[28,77] In addition, von Sonntag discusses the influence of hydrated electrons on DNA. He noted that they can induce base damage, whereby the rate constants of hydrated electrons to DNA bases are in the order of 10^9 to 10^{10}.[28] These reaction rates of OH-radicals with DNA are clearly higher than those for amino acids, eventually explaining the difference in radiation damage detected in this study. It is therefore proposed that through the present amino acids and especially the protein, the reaction rates of both electrons[28,71,72] and other free radicals[73,75,76] in ambient water are changed as compared to DNA. Therefore, different radiation damage results were observed for amino acids and proteins under NAP conditions as compared to DNA.

This, in combination with a decreased likelihood for direct damage in hydrated amino acids compared to the dry samples, may explain the observed overall decrease in susceptibility to radiation. For example, the ambient water and related hydration shells behave differently than liquid (bulk) water. This could modify the charge transfer and thus lead to the exclusion of charged particles from the sample surface. The ambient water could provide an alternative reaction pathway for these particles, as for example by quickly transporting ejected electrons away from the sample surface, so that further processes (probably happening under UHV) cannot take place under NAP conditions. During NAP measurements of amino acids, damage at the amino- and carboxyl-groups (similar to the damage detected under UHV) is detected but (almost) no alterations of the side-chain can be seen. This could suggest a stronger effect of the presence of water and the respective reactive particles to the amino- and carboxyl-groups rather than the side-chains of the amino acids, since the relative contributions from C1s, and especially simple C–C bonds that only occur in the side chains, increase over time (see Fig. 9, left column C1s normalized peak areas). However, a desulphuration though the cleavage of the C–S bond in the side-chain of cysteine was, once again, detected under NAP conditions. Thus, relevant radiation damage can occur in the side-chain if relevant electron-rich groups (like S–H) are present. A more detailed explanation could be expected from an in-depth assessment of the underlying chemical reaction by time resolved experiments or simulational methods.

For the G5P protein, no clear changes in the spectral features upon irradiation under NAP conditions were detected. The breakage of peptide bonds cannot be stated from the irradiation results. In addition, also the cleavage at C- or N-terminal sites of the protein as well as respective damage to the side-chain cannot be perceived. For the model protein G5P it was already proven that radiation damage occurs in the presence of water.[15] During SAXS measurements, aggregation and cross-linking dominate in aqueous solutions, while fragmentation dominates when hydroxyl-radical scavengers are present. Here, conformational changes of the protein and loss of function were proposed. Nevertheless, the radiation damage of measurements in solution (where the probed molecule is fully dissolved) and measurements under a water atmosphere (where the probed molecule remains in solid form on the sample holder and is not dissolved) are not necessarily comparable. In solution, various factors like pH, concentrations and co-solutes as well as the probed molecules movement have to be considered. For example, the peptide backbone of protein can be protected inside the molecule when solvated.

It must be kept in mind that no individual, isolated molecules are being considered in this study. Here, the molecules are close to each other, which could also represent the conditions in a physiological, crowded environment. In particular, an amino acid-rich environment can mimic the environment within a protein: here, the side-chains of the amino acids are in close vicinity to each other, enabling interactions between them. Thus, in this study, reactions between the individual molecules are very likely, if not the most probable. In this context, the examination of S2p spectra is particularly relevant because the sulphur bridges *via* cysteine side chains are crucial for the three-dimensional structure of proteins in general, among other things. For this reason, cysteine was also included in this study even though G5P itself does not contain any sulphur bridges. The particularly electron-attracting sulphur in the side chain is predisposed to be attacked by reactive particles,[64] which lead to the cleavage of the S–H – group, as described above. It is therefore also suspected that sulphur is cleaved from cysteine residues in the protein. Unfortunately, no precise statement can be made based on the XPS spectra, because the S-content in the protein is too low to generate accurate S2p spectra or rather the respective SNR is too high to monitor the signal. In this experimental set-up the relative amount of water is lower then in a biological (cellular) environment. A first attempt to mimic the presence of water in such an environment was the application of near-ambient pressure conditions. In addition to water and DNA, counterions, other proteins like histones and other co-solutes are present in nuclei of mammalian cells. Some of them are known to alter the damage yield to DNA against OH-radical attacks or altering the damage efficiency of low-energy electrons upon irradiation.[10] Especially the binding of proteins to DNA can modify the reactivity of nucleotide radicals[4] and generally alter charge migration through the DNA double-strand. But, even despite the presence of DNA-binding proteins, DNA integrity cannot be guaranteed, as the tendency for radiation-induced protein–DNA cross-links increases.[12] These cross-links occur predominantly under low-oxygen conditions, as often are present in cancer cells.[9] This type of damage is difficult to repair for the cell and can lead to mutations and loss of function. Thus, the presence of these other molecules and co-solute could also generally influence the radiation damage to proteins.[15] In cells, the oxidative modification of proteins marks them for degradation through proteases, enabling fast repair or replacement of damaged proteins. Furthermore, the accumulation of oxidized proteins in cells is considered a marker for ageing processes, oxidative stress and several pathological states.[68]

To advance radiation therapy (and to improve radiation protection), a comprehensive understanding of the mechanisms involved in the degradation of biomolecules upon ionization and radical attacks has to be achieved and further

investigated on. Additionally, experiments for the investigation of the complex of ssDNA and G5P to further examine the complicated interaction between these biomolecules are needed, for example with XPS under UHV and NAP conditions but also under varying oxygen conditions. Furthermore, the application of other (heavy) particles to compare the respective radiation damage could deliver valuable results.

5. Conclusions

To summarize, here X-ray radiation damage to amino acids, short peptides and proteins was analysed. A comparison of ultra-high vacuum (UHV) and near-ambient pressure (NAP) X-ray photoelectron spectroscopy (XPS) experimental data to determine the effect of the presence of water to the radiation response of the named biomolecules was performed. The zwitterionic nature of both the pure amino acids as well as the small peptides in the solid state was clearly identifiable from the presence of signals from protonated amino- and deprotonated carboxyl-groups. Upon irradiation under dry conditions, all samples showed chemical degradation and thus radiation damage at respective subunits like deamination, decarboxylation, demethylation and desulphuration. Various free-radical induced mechanisms were discussed, whereby a core-level ionization of the probed molecules is the principal ionization channel. Secondary reactions can occur inter- or/and intramolecularly, initiated by resulting low-energy electrons (LEE) and free radicals.[9,45] A tendency from the zwitterionic configuration towards more neutral species was detected for the single amino acids. In addition, a formation of peptide bonds was proposed. Opposed to this, the breakage of peptide bonds was detected for short peptides and the model protein, gene-V protein, next to fragmentations at the side-chains. Under NAP conditions, a water atmosphere was applied allowing for additional indirect damage pathways derived from water radiolysis. Here, no increase in damage was detected for all samples as compared to dry conditions which was surprising and unexpected since the same experimental set-up used on DNA delivered strongly increased damage and changed damage pathways under the presence of water.[9] Possible explanations for the discrepancy between DNA and protein experiments were discussed, proposing the exclusion of charged particles from the sample surface. Most likely, altered deexcitation pathways and lower reaction rates of reactive particles like electrons and other free radicals derived from water radiolysis under the presence of amino acids, peptides and the protein are the reason behind these anticipated charges and the different results as compared to DNA. Nevertheless, additional investigations of the damage pathways under the presence of water at the sample surface is needed in the future, since the chemical degradation of complex molecules and especially proteins like G5P remain difficult to decipher in detail from the NAP spectra. Generally, the versatility of XPS was proven in this study, with the *in situ* radiation damage and detection of elemental composition of the studied molecules. Here, especially the distinction of amino acids through the presence of photoemission features from functional groups in complex amino acid side-chains and the even more complex protein, consisting of 87 amino acids, must be highlighted. The data from radiation damage to proteins that interact with DNA under biological conditions are highly relevant for the treatment of cancer with radiotherapy, but also for other research fields like astrobiology and the beginning of life itself.

Author contributions

DCH and MBH conceived the study together. DCH expressed and purified the protein, prepared the samples, analysed and discussed results and wrote the paper with contributions from the other authors. JR performed the XPS vacuum measurements and contributed to the interpretation of the data. PMD performed NAP-XPS measurements and contributed to the interpretation of the data. HS contributed to the discussion. MBH contributed to the interpretation and the discussion.

Conflicts of interest

There are no conflicts to declare.

Data availability

The data, codes and materials that support the findings of this study are available from MBH upon request.

Supplementary information (SI): with additional spectra, simulation results, and information about the fitting procedure. See DOI: **https://doi.org/10.1039/d5cp01887k**.

Acknowledgements

The authors thank Dirk Michel for the kind support with the SciFLEX for spotting the samples and Petr Slavíček for valuable discussions. The authors acknowledge funding by Deutsche Forschungsgemeinschaft DFG (German Research Foundation) under project number 442240902 (HA 8528/SE 2999).

References

1 L. Sanche, *Nature*, 2009, **461**, 358–359.
2 M. B. Hahn, *J. Phys. Commun.*, 2023, **7**, 042001.
3 S. Ptasinska, *et al.*, *J. Chem. Phys.*, 2008, **129**, 065102.
4 X. Peng, Y. Z. Pigli, P. A. Rice and M. M. Greenberg, *J. Am. Chem. Soc.*, 2008, **130**, 12890–12891.
5 S. R. Rajski, S. Kumar, R. J. Roberts and J. K. Barton, *J. Am. Chem. Soc.*, 1999, **121**, 5615–5616.
6 S. R. Rajski and J. K. Barton, *Biochemistry*, 2001, **40**, 5556–5564.
7 B. Giese, *Acc. Chem. Res.*, 2000, **33**, 631–636.
8 B. Giese, *Curr. Opin. Chem. Biol.*, 2002, **6**, 612–618.
9 M. B. Hahn, P. M. Dietrich and J. Radnik, *J. Commun. Chem.*, 2021, **4**, 1–8.

10 M. B. Hahn, S. Meyer, H.-J. Kunte, T. Solomun and H. Sturm, *Phys. Rev. E*, 2017, **95**, 052419.
11 M. Spotheim-Maurizot and M. Davidkova, *Mutat. Res., Fundam. Mol. Mech. Mutagen.*, 2011, **711**, 41–48.
12 C. C. Bjorklund and W. B. Davis, *Biochemistry*, 2007, **46**, 10745–10755.
13 S. Krasnokutski, K. Chuang and C. E. A. Jäger, *Nat. Astron.*, 2022, **6**, 381–385.
14 C. L. Hawkins and M. J. Davies, *Biochim. Biophys. Acta, Bioenerg.*, 2001, **1504**, 196–219.
15 D. C. Hallier, G. J. Smales, H. Seitz and M. B. Hahn, *Phys. Chem. Chem. Phys.*, 2023, **25**, 5372–5382.
16 T. Solomun, H. Sturm, R. Wellhausen and H. Seitz, *Chem. Phys. Lett.*, 2012, **533**, 92–94.
17 T. Solomun, L. Cordsmeier, D. C. Hallier, H. Seitz and M. Hahn, *J. Phys. Chem. B*, 2023, **127**, 8131–8138.
18 M. B. Hahn, *et al.*, *J. Phys. Chem. B*, 2015, **119**, 15212–15220.
19 N. Ashton, E. Bolderson, L. Cubeddu, K. O'Byrne and D. Richard, *BMC Mol. Biol.*, 2013, **14**, 9.
20 J. Coleman and J. Oakley, *CRC Crit. Rev. Biochem.*, 1980, **7**, 247–289.
21 M. M. Skinner, *et al.*, *Proc. Natl. Acad. Sci. U. S. A.*, 1994, **91**, 2071–2075.
22 G. Olah, D. M. Gray, C. W. Gray, D. L. Kergil, T. R. Sosnick, B. L. Mark, M. R. Vaughan and J. Trewhella, *J. Mol. Biol.*, 1996, **249**, 576–594.
23 J. Stevens, A. de Luca, M. Pelendrtitis, G. Terenght, S. Downes and S. Schroeder, *Surf. Interface Anal.*, 2013, **45**, 1238–1246.
24 M. Spotheim-Maurizot and M. Davidkova, *J. Phys.: Conf. Ser.*, 2010, **261**, 012010.
25 C. S. Bury, I. Carmichael, J. E. McGeehan and E. F. Garman, *Radiat. Phys. Chem.*, 2016, **128**, 118–125.
26 M. B. Hahn, S. Meyer, M.-A. Schröter, H. Seitz, H.-J. Kunte, T. Solomun and H. Sturm, *Phys. Chem. Chem. Phys.*, 2017, **19**, 1798–1805.
27 E. L. Alpen, *Radiation Biohphysics*, Academic Press, Revised edn, 1998.
28 C. von Sonntag, *Free-Radical-Induced DNA Damage and Its Repair*, Springer, 2006.
29 T. Ito, S. C. Baker, C. D. Stickley, J. G. Peak and M. J. Peak, *Int. J. Radiat. Biol.*, 1993, **63**, 289–296.
30 J. F. Ward, in *DNA Damage and Repair*, ed. J. A. Nickoloff and M. F. Hoekstra, Humana Press, Totowa, NJ, 1998, pp. 65–84.
31 B. Abel, U. Buck, A. L. Sobolewski and W. Domcke, *Phys. Chem. Chem. Phys.*, 2011, **14**, 22–34.
32 M. Mucke, *et al.*, *Nat. Phys.*, 2010, **6**, 143–146.
33 X. Pan, P. Cloutier, D. Hunting and L. Sanche, *Phys. Rev. Lett.*, 2003, **90**, 208102.
34 E. Alizadeh, T. Orlando and L. Sanche, *Annu. Rev. Phys. Chem.*, 2015, **66**, 379–398.
35 D. Becker and M. D. Sevilla, in *Radiation Research*, ed. J. T. Lett and W. K. Sinclair, 1993, 17, pp. 121–180.
36 I. Standard, ISO 15472:2010, Geneva Switzerland., 2010, 2nd edn.
37 M. KjÃ¦rvik, K. Schwibbert, P. Dietrich, A. Thissen and W. E. S. Unger, *Surf. Sci. Spectra*, 2018, **50**, 556–1000.
38 D. I. Patel, D. Shah, S. Bahr, P. Dietrich, M. Meyer, A. Thißen and M. R. Linford, *Surf. Sci. Spectra*, 2019, **26**, 014026.
39 P. Dietrich, D. R. Baer, F. Mirabella and A. Thissen, *Surf. Sci. Spectra*, 2025, **32**, 013001.
40 M. Wojdyr, *J. Appl. Crystallogr.*, 2010, **43**, 1126–1128.
41 R. Hesse, T. Chassé, P. Streubel and R. Szargan, *Surf. Interface Anal.*, 2004, **36**, 1373–1383.
42 S. Agostinelli, *et al.*, *Nucl. Instrum. Methods Phys. Res., Sect. A*, 2003, **506**, 250–303.
43 J. Perl, J. Shin, J. Schumann, B. Faddegon and H. Paganetti, *Med. Phys.*, 2012, **39**, 6818–6837.
44 J. M. Zutta Villate and M. B. Hahn, *Eur. Phys. J. D*, 2019, **73**, 95.
45 Y. Zubavichus, *et al.*, *Radiat. Res.*, 2004, **116**, 346–358.
46 R. Nicklin, *et al.*, *J. Phys. Chem. C*, 2015, **119**, 26566–26574.
47 K. Bomben and S. Dev, *Anal. Chem.*, 1988, **60**, 1393–1397.
48 K. Takenaka, K. Cho, Y. Setsuhara, M. Shiratanim, M. Sekine and M. Hori, *J. Phys.: Conf. Ser.*, 2013, **441**, 012001.
49 A. Artemenko, A. Shckukarev, P. Stenclova, T. Wagberg, J. Sergvald, X. Jua and A. Kromka, *DMSRE30*, 2021, **1050**, 012001.
50 K. Uvdal, P. Bodö and B. Liedberg, *J. Colloid Interface Sci.*, 1991, **149**, 162–173.
51 A. Ihs, B. Liedberg, K. Uvdal, C. Törkvist, P. Podö and I. Lundström, *J. Phys. Chem. B*, 1990, **140**, 192–206.
52 G. Tzvetkov and F. Netzer, *J. Electron Spectrosc. Relat. Phenom.*, 2010, **182**, 41–46.
53 W. Zhang, V. Carravetta and O. E. A. Plekan, *J. Phys. Chem.*, 2009, **131**, 035103.
54 H. Abdoul-Carime and L. Sanche, *Radiat. Res.*, 2003, **160**, 86–94.
55 H. Abdoul-Carime and L. Sanche, *J. Phys. Chem. B*, 2004, **108**, 457–464.
56 in *The XPS of Polymers Database*, ed. G. Beamson and D. Briggs, Surface Spectra Limited, Manchester, UK, 1st edn, 2000.
57 D. Shah, D. I. Patel, S. Bahr and P. Dietrich, *Surf. Sci. Spectra*, 2019, **26**, 024003.
58 M. Bozack, Y. Zhou and S. Worlex, *J. Chem. Phys.*, 1994, **100**(11), 8392–8398.
59 R. Wilks, J. MacNaughton, H.-B. Kraatz, T. Regier, R. Blyth and A. Moewes, *J. Phys. Chem. A*, 2009, **113**, 5360–5366.
60 M. Lehmann, J. Verbist, W. Hamiltorn and T. Koetzle, *J. Chem. Soc., Perkin Trans. 2*, 1973, 133.
61 in *Hydrogen Technology. Green Energy and Technology*, ed. D. Schild and A. Léon, Springer, Berlin, Heidelberg, 2008.
62 J. Bergès, P. Trouillas and C. Houée-Levin, *J. Phys.: Conf. Ser.*, 2011, **261**, 012003.
63 A. Gatin, I. Billault, P. Duchambon, G. Van-der Rest and C. Sicard-Roselli, *Free Radical Biol. Med.*, 2021, **162**, 461–470.
64 H. Abdoul-Carime and L. Sanche, *Radiat. Res.*, 2002, **158**, 23–31.
65 W. Lange, M. Jirikowsky and A. Benninghoven, *Surf. Sci.*, 1984, **136**, 419–436.
66 J. F. Ward, in *Progress in Nucleic Acid Research and Molecular Biology*, ed. W. E. Cohn and K. Moldave, Academic Press, 1988, vol. 35, pp. 95–125.

67 P. Cloutier, C. Sicard-Roselli, E. Echer and L. Sanche, *J. Phys. Chem. B*, 2007, **111**, 1620–1624.
68 E. R. Stadtman, *Annu. Rev. Biochem.*, 1993, **62**, 797–821.
69 E. Wang, *et al.*, *Nat. Commun.*, 2020, **11**, 1–7.
70 T. Jahnke, *et al.*, *Chem. Rev.*, 2020, **120**, 11295–11369.
71 C. Richter, D. Hollas and C. Saak, *et al.*, *Nat. Commun.*, 2018, **9**, 4988.
72 R. Braams, *Radiat. Res.*, 1966, **27**, 319–329.
73 M. Enescu and B. Cardey, *ChemPhysChem*, 2006, **7**, 912–919.
74 M. Hoffmann and E. Hayon, *J. Phys. Chem.*, 1973, **77**, 990–996.
75 T. Masuda, S. Nakando and M. Kondo, *J. Radiat. Res.*, 1973, 339–345.
76 T. Schaefer, Y. Zhang, L. He, O. N. Ventura and H. Herrrmann, *Phys. Chem. Chem. Phys.*, 2022, **24**, 11054–11065.
77 A. Ly, J. Aguilera and J. Milligan, *Radiat. Phys. Chem.*, 1993, **76**, 982–987.

